Dynamic properties of a pedestrian bridge

Case study of the bridge passing Roslagsbanan at Fysikcentrum.

Andreas Andersson

Preface

This report comprise dynamic analyses and measurements of a pedestrian bridge situated in Stockholm near KTH. The report is a part of the post-graduate course "Advanced Structural Dynamics, Modelling and Measurements". The field measurements were carried out on the 5th of October 2006 by the course attendants under supervision of Claes Kullberg, Stefan Trillkott and associate professor Raid Karoumi at the department of civil and architectural engineering. The instrumentation used in the field measurements were provided by KTH and LTU.

Stockholm, November 2006

Andreas Andersson

Abstract

The aim of this report is to study the dynamic properties of a pedestrian bridge. For this purpose, field measurements have been performed in order to determine the natural frequencies, damping ratios and mode shapes of the bridge. The modal analysis of the measured data has been performed using the commercial software ARTeMIS. The static system of the bridge has been evaluated using the information gained from the modal analysis along with finite element modelling in the commercial software SOLVIA-03.

When comparing the results from the FE-model with the modal analysis based on the measured response, it was found that the bearing friction had large influence on the results, mainly considering the natural frequency. The degree of restraint in the column was also found to be of great importance. The column is founded on a group of piles resulting in a significant elastic restraint rather that fully clamped.

Preliminary FE-analysis using a simplified 3D beam element model regarding the elastic restraint of the column was found to give rather sufficient results regarding natural frequencies and mode shapes. A refined 3D solid element model was later established mainly to better account for the geometry variation.

When identifying the static manner of action the bridge is subjected to, the mode shapes estimated from the modal analysis played a significant role. For reasonable proper boundary conditions in the FE-analysis the same mode shape could be identified from both modal analysis and FE-analysis. The influence of the parameters in the FE-model could then be evaluated to correspond to the modal analysis regarding natural frequency. The FE-analysis also provided information where physical modes should appear in the modal analysis. The first 10 structural modes, involving vertical, transversal and torsion modes were found and paired between the FE-analysis and the modal analysis.

The natural frequencies contained in the measured signals were found to be estimated within $0.5 - 1.0\%$. The estimation of the damping ratio on the other hand, contained large uncertainties although the average damping ratio was found at about 1 %. This was also confirmed from analysis of transient excitation. The damping ratio was then evaluated using the decay of a single frequency.

As the lowest natural frequencies were obtained under 3.5 Hz, acceleration analysis must be performed for these frequencies according the Swedish Road Regulations, Bro 2004. The analysis was performed by the bridge constructor and showed allowable values using the damping ratio 0.6 %. Using the estimated damping 1 % increase the safety of acceleration criteria.

Keywords: Field measurements, Dynamics, Finite Element Methods, FEM, Modal analysis, ARTeMIS, Pedestrian bridge, Post tension cables.

Table of Contents

1 Introduction

1.1 General aims and scope

The aim of this report is to study the dynamic properties of a pedestrian bridge. This has been done by performing field measurements. The results, primary consisting of acceleration responses from the bridge, have been analyses using modal analysis. The results of the analysis consist of mode shapes with estimation of corresponding natural frequencies and damping ratios. The results are further compared with FE-models to gain more information on the structural behaviour of the bridge, both in a static and dynamic manner.

1.2 Description of the bridge

The pedestrian bridge studied in this report is a post-stressed concrete girder bridge in two spans, see Figure 1.1. Some general assembly drawings are found in Appendix A. The spans are 34.75 m each and the support at the middle consists of a 9 m long column. The mid-column is continuous with the bridge deck and supported on a group of plies, founded on solid rock. The piles are approximately 4 m in length. The column has a solid rectangular cross-section 1.8·0.8 m. The bridge deck is simply supported on bearings at both abutments. The north abutment is founded on solid rock and the south is founded on a group of piles with approximately 5 m length. The cross-section of the bridge deck, described in Figure 1.2 varies as presented in Figure 1.3.
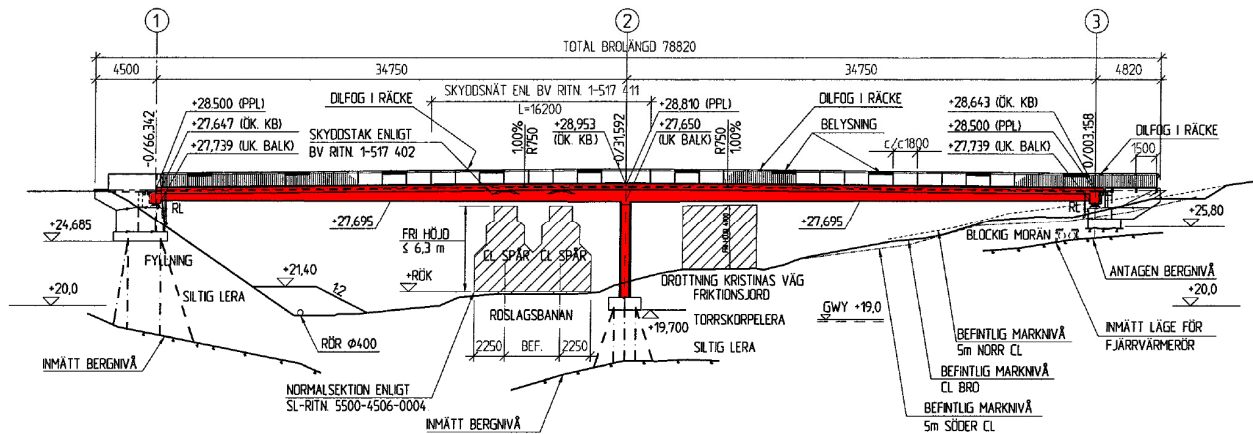

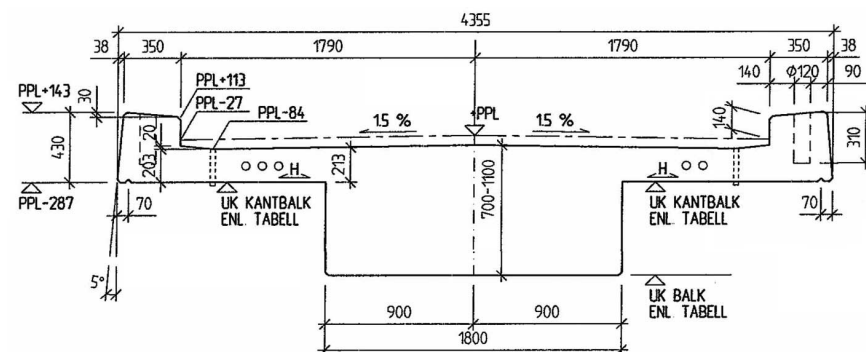Figure 1.1:   Elevation of the bridge, marked in red.

Figure 1.2:   Cross-section of the bridge deck, variable parameters PPL, UK KANTBALK and UK BALK are presented in Figure 1.2 – Figure 1.4.
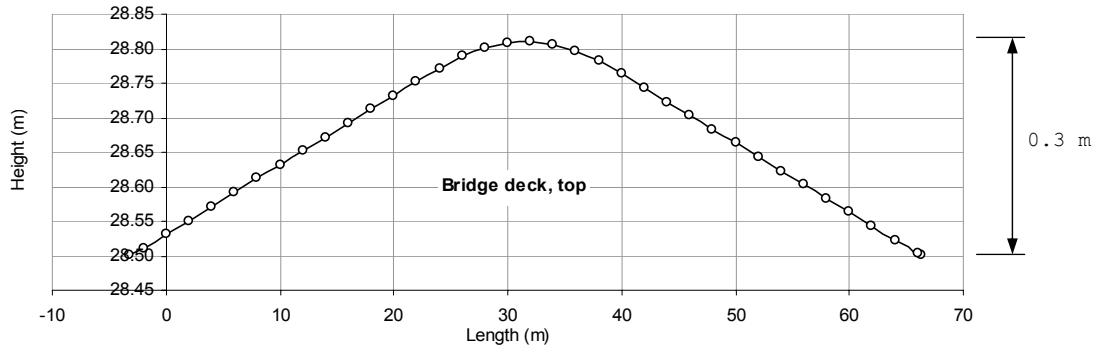
1

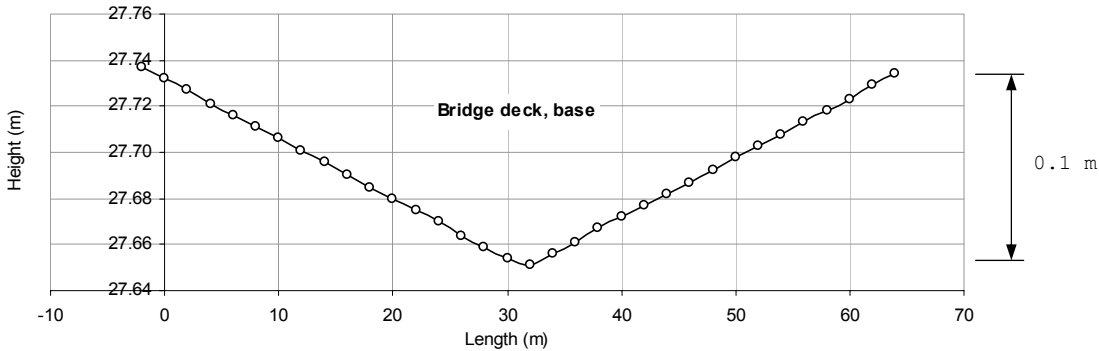Figure 1.3:   Varation of the bridge deck top, denoted `PPL`.

Figure 1.4:   Varation of the bridge deck base, denoted `UK BALK`.
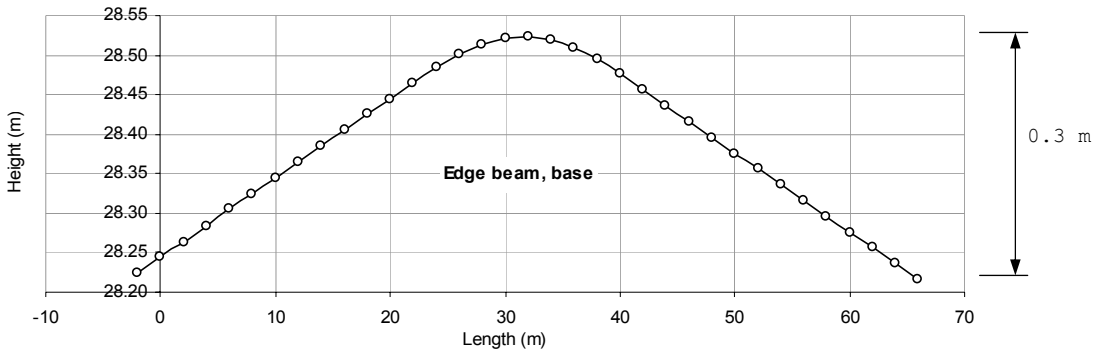
Figure 1.5:   Varation of the bridge deck edge beam, denoted `UK KANTBALK`.

The bridge deck consists of concrete class K45 and the column of concrete class K40. The reinforcement quality class is Ks60S. The bridge consists of fourteen tendons of the type VSL 12ϕ16. Six tendons are continuous along the entire bridge. The remaining eight are anchored between the abutment and the column.

1.3   A brief literature survey

The following subchapter contains a brief literature review on pedestrian induced vibrations. A thoroughly review of the subject has been done by [8].

In later years, the trend of bridge design has resulted in more slender constructions. This has been possible due to development of refined construction materials and method as well as

increased use of advanced design tools to optimise the structure. This trend has been amplified by the demand of aesthetic design in form of architectural design competitions. A slender design often results in increased influence of dynamic load effects. The decrease in mass results in lower energy to excite the structure. In the case of pedestrian bridges, several cases of excessive vibrations have been discovered. The most well known case is probably the Millennium bridge in London, where unexpected dynamic responses from pedestrians has resulted in revised design codes.

In order to determine the risk of undesired vibrations in pedestrian bridges, the dynamic interaction between pedestrians and the bridge must be identified. The most common way is to isolate the response from a single pedestrian. Pedestrians in motion induce vibrations in three directions, vertical, horizontal-lateral and horizontal-longitudinal. In most cases the vertical component is of greatest interest, since it contains the highest energy. The amount of energy depends on several walking parameters, such as the step length, moving velocity, peak force and contact time [8]. In the case of slow or normal walking, the load has found to be rather constant over time, resulting in a response similar to a moving point load. In the case of running, a more triangular amplitude function is obtained with a shorter duration. This results on the other hand in an increased amplification, commonly three times the static load obtained from slow walking.

It has been shown that the walking pace is normal distributed along 2 Hz, as presented in Figure 1.6. According to The Swedish design codes for bridges [6], dynamic acceleration calculations must be performed on pedestrian bridges having a resonance frequency lower than 3.5 Hz.
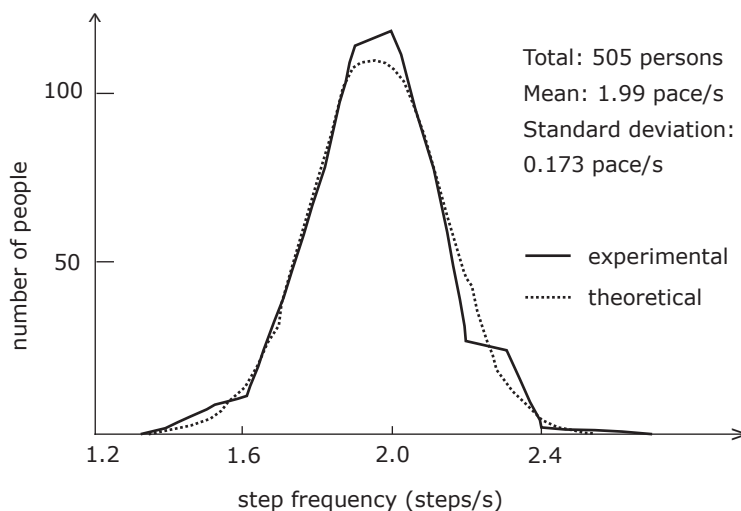
Figure 1.6:   Normal distribution of pacing frequencies for normal walking, reproduced from [8].

The influence of synchronized walking often has larger impact on a bridge rather than the amplification of running pedestrians. This is due to that synchronized walking is more difficult to achieve at higher step frequencies. Although the vertical force induced by pedestrians is far larger than the transversal components, excessive vibration due to lateral induced pedestrian load has been obtained, i.e. for the Millennium bridge in London, [2].

2 Finite Element modelling

2.1 Describing the models

Two different FE-models have been established, a simplified 3D beam element model for rough estimation of the static system as well as the dynamic properties, and a detailed 3D solid model that in more detail accounts for the correct boundary conditions and cross-sectional properties.

2.1.1 3D beam element model

The beam elements are formulated using Bernoulli-Euler theory, which is based on the assumption that plane sections normal to the axis remains plane after deformation. Shear deformations are added to the bending deformations and are based on equivalent shear areas of the cross-section in the directions of principal moments of inertia. The dynamic properties of the bridge can with good accuracy be modelled using the beam element model, possibly even in torsion.

The static system of the FE-model is presented in Figure 2.1. The elastic restraint of the column is accounted for by modelling the entire group of piles, as in Figure 2.2.
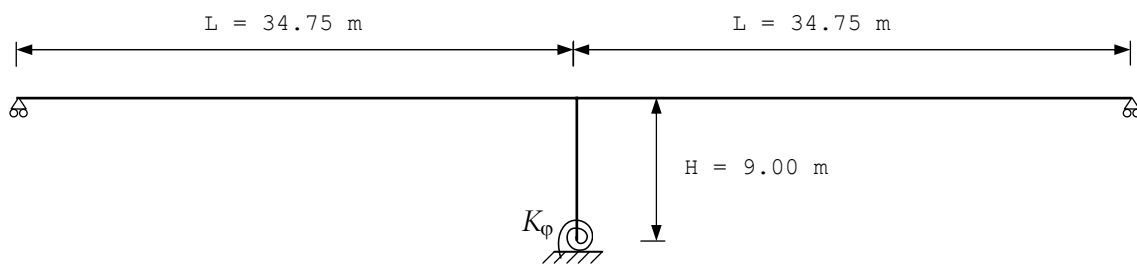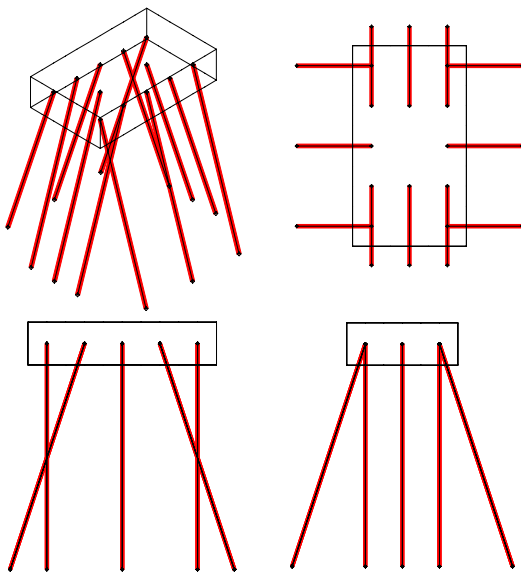

Figure 2.1: Static system of the bridge.

Figure 2.2: Group of piles in the FE-model.

General cross-section parameters can be described, to account for edge beams and variation in dimensions along the bridge. The established beam element model is however simplified to a constant T-shaped cross-section as shown in Figure 2.3.


```
SCALE ├───────┤ 0.50
◇  Stress point
WTOP=4.350
D=0 9800
T1=0.2700
T2=1.800
RI=1.409
SI=0.2108
TI=2.197
AREA=2.452
SPAREA=1.174
TPAREA=1.764
SSC=0.000
TSC=0.2202
```
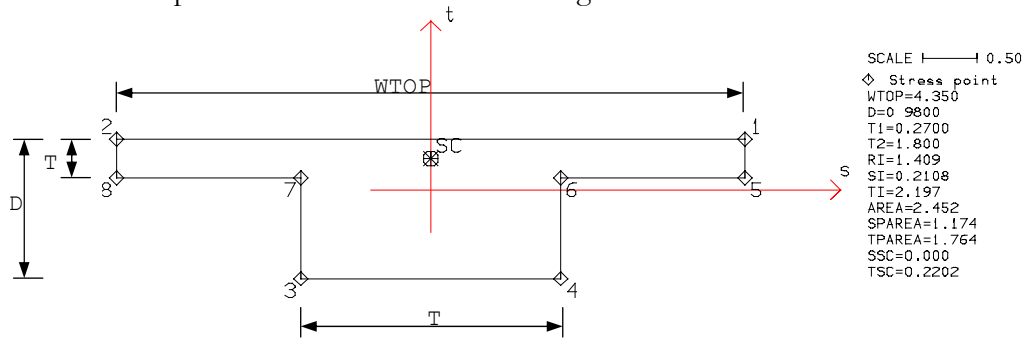
Figure 2.3:   Constant T-shaped cross-section used in the beam element models.

The influence of the post-tendons has been studied using the beam element model. In the FE-system SOLVIA-03 post-tendons can be accounted for in terms of equivalent loads. The curve of the tendon described in Figure 2.4 is defined in the FE-model. The input parameters, based on the original construction drawings are the tensile strength $\sigma_{0.2} = 1550$ MPa, the tendon force $F = 2372$ kN/cable corresponding to 85 % of $\sigma_{0.2}$. The friction loss coefficient is $\mu = 0.18$ and the profile factor is $k = 0.0022$.
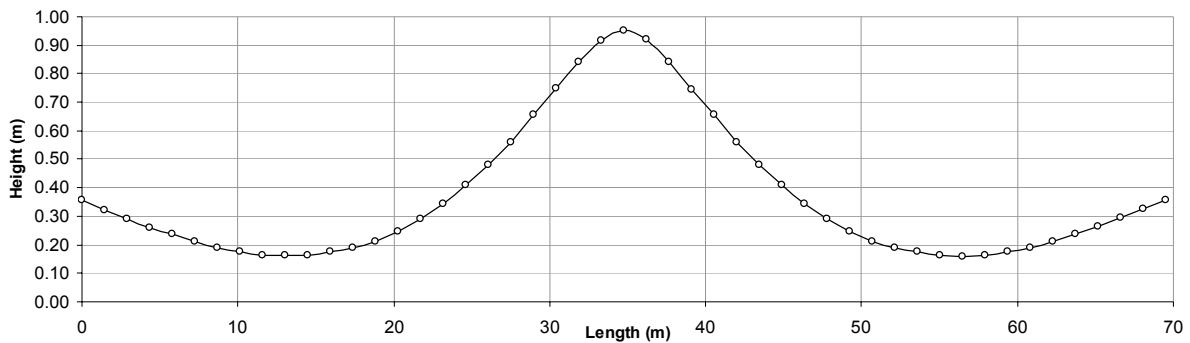
Figure 2.4:   Averages curve describing the tendons.

The results of the FE-analysis taking into account the post-tendons were shown not to change the natural frequency noticeably.

2.1.2   3D beam solid element model

The 3D solid element model consists of 8-node solid element with the element size 0.3 m. The cross-section is presented in Figure 2.5. The cross-section varies linear from the abutments to the mid-column similar to presented in Figure 1.3 – Figure 1.5. The abutment is modelled as shown in Figure 2.5, where bearings are distanced 3 m apart. The bearings are initially constraint in transversal direction. However, during model calibration it was found that bearing friction longitudinal to the bridge is significant, which has been modelled as a constraint in this direction.

The column is modelled as a rectangular beam element rigidly constraint to the bottom of the bridge deck as shown in Figure 2.6.

Figure 2.5:   Cross-section in the 3D solid element model.
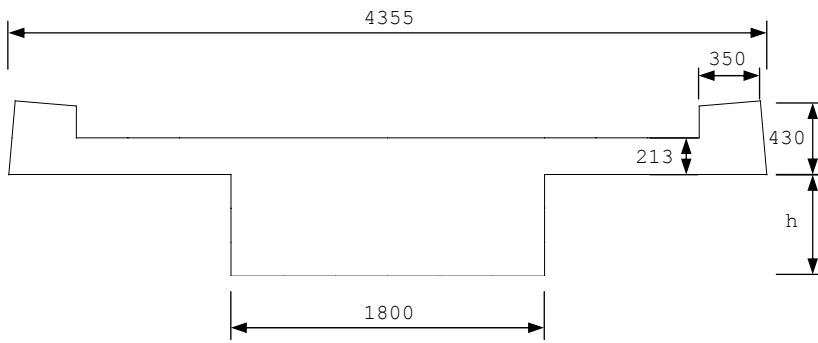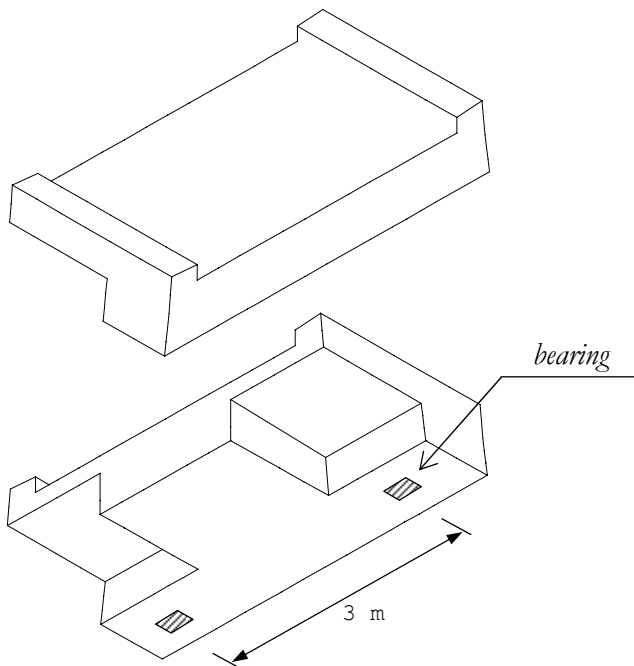

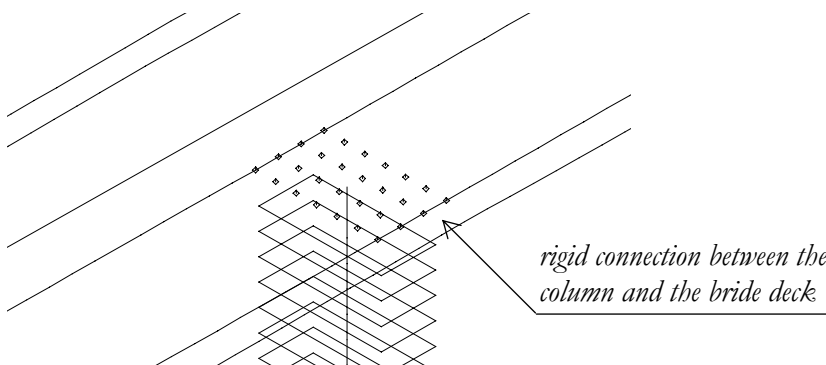Figure 2.6:   Cross-section in the 3D solid element model.

Figure 2.7:   Connection with the column at the bridge deck.

2.2 Eigenvalue analyses

Eigenvalue analysis has been performed to calculate the natural frequencies and corresponding modes shapes. Some rough estimation of the expected modes can be done by handbook formulas as

$$f = \frac{\mu_n^2}{2\pi} \sqrt{\frac{EI}{mL^4}} \tag{2.1}$$

where μ_n is a factor depending on the boundary conditions. For a bi-pinned beam $\mu_n = n\pi$ for mode number n. For a uni-clamped beam the approximation $\mu_n = (4n+1)\pi/4$ may be used for low n. The bi-pinned boundary conditions can be related to the anti-metric modes of the bridge and the uni-clamped to the symmetric modes. The anti-metric modes are in general more influenced by the rigidity in the column. The results from the simple handbook formulas shows very good agreement with results estimated from measured data.

Table 2.1: Natural frequencies from vertical bending modes, comparions between handbook formulas and measured data.

mode:	bi-pinned	bi-pinned/ measured	uni-clamped	uni-clamped/ measured
1	1.41	0.79	2.20	0.82
2	5.63	1.00	7.12	0.98
3	12.66	-	14.86	1.03

Eigenvalue analysis of the FE-models has been performed. Any difference between the 3D beam element model and the 3D solid element model depends almost solely on difference in cross-sectional properties and boundary conditions, at least regarding pure bending modes. As for the torsion modes on the other hand, the Bernoulli-Euler theory may not always result in accurate results. A comparison of frequency and mode shapes between the 3D solid element model and the modal analysis based on measured data are presented in Appendix D.

Eigenvalue analyses are in general independent on external loads, as implied in Equation 2.1. In some cases however, the external load may be significant, such as in a taut string. In order to account for such external loads, a RESTART analysis has been performed in the FE-analysis.

3 Field measurements

3.1 Aims and scope

The field measurements were carried out on the 5th of October 2006. The aim of the field measurements was to measure dynamic response during different loadings in order to gain information of the structural behaviour of the bridge.

3.2 Instrumentation

The instrumentation used during the field measurements were

- 5 accelerometer using Micro Electro Mechanical Systems (MEMS) technology, provided by KTH

- 1 Linear Variable Differential transformer (LVDT) measuring displacement, provided by KTH

- 1 Ultra-Low Frequency Vibration Gauge, measuring either acceleration, speed or displacement, provided by LTU

- 1 Laser gauge, measuring displacement, provided by LTU

Figure 3.1: Assembly of accelerometers, MEMS accelerometer on the left mounted to a heavy steel wieght, Ultra-Low Frequency Gauge on the right. The lower gray box is a power supply consisting of one 9V battery.

Figure 3.2:   Position of the LVDT in contact with the bottom of the bridge deck.
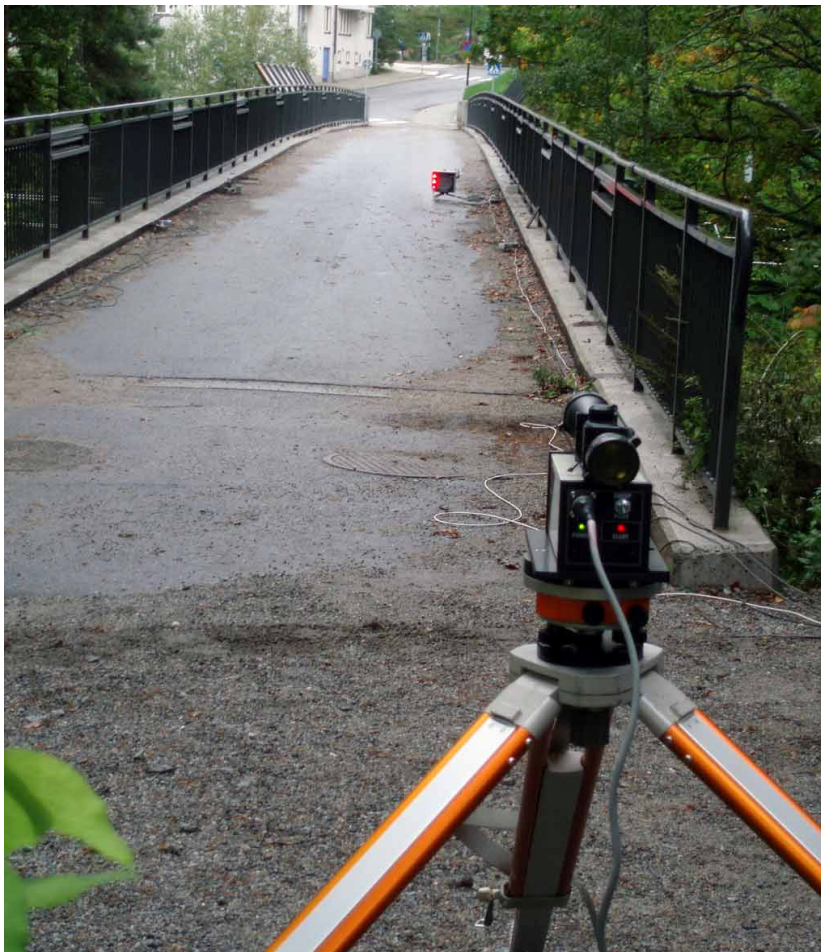

Figure 3.3:   Assembly of the laser. A laser beam is directed to a reviever positioned on the bridge. The laser measures displacement both vertical and transversal simultaneously.

3.3   Measurement procedures

The measurements are described in mode detail in Appendix B. The primary strategy of the measurements was to later perform a modal analysis to evaluate the mode shapes of the bridge. For this purpose, a large number of measurement positions must be covered in order to achieve decent mode shapes in the later analysis. Using a limited number of gauges, several measurements can be performed where some gauges are fixed throughout all measurements and some are moved into different positions. The fixed ones work as reference gauges to relate different measurements with each other. In this way, an arbitrary amount of points on the bridge can be measured with a limited number of gauges. In this case thirteen different measurements were performed, where nine consisted of ambient pedestrian excitation. During these measurements, two accelerometers were placed in different positions.

When analysing low-frequency vibrations, a high measure time must be used, in order to measure sufficiently many cycles. The time duration is therefore dependent on the lowest mode, in this case about 1 Hz. It is recommended that at least 500 periods of the lowest frequency is measured, meaning a measuring time of 10 min, which was used.

4   Analysing field measurements

4.1   Modal analysis using ARTeMIS

The modal analysis software ARTeMIS has been used for evaluation of the natural modes of the bridge. Two different evaluation methods have been carried out, the Frequency Domain Decomposition (FDD) and the Stochastic Subspace Identification (SSI).

4.1.1   Frequency domain decomposition

The FDD technique is based on an approximate decomposition of the system response into a set of independent single degree of freedom (SDOF) systems. Each mode is described by one SDOF. The decomposition is performed by decomposing each of the estimated spectral density matrices. The FDD technique can be divided in the following steps:

1) Estimate spectral density matrices from the raw time series data

2) Singular value decomposition (SVD) of the spectral density matrices

3) In multiple data sets, the singular values are averaged over all data sets in increasing mode order

4) Peak-pick of the singular values, either from the averaged values or for each data set separately

The peak-pick is carried out manually in the program. Damping ratios can be estimated using the Enhanced Frequency Domain Decomposition (EFDD). The mode shapes identified by the FDD technique are used in identifying SDOF Bell functions. The FDD mode shape is used as a reference vector a correlation analysis based on the Modal Assurance Criterion (MAC). The MAC value controls the width of the SDOF Bell function in the frequency domain. The damping ratio as well as the natural frequency is estimated by transforming the SDOF Bell function into time domain along with regression analysis.

4.1.2   Stochastic subspace identification

The SSI technique is based on a parametric model that is fitted to the measured response in time domain. The time domain modal identification technique can be formulated as

$$\hat{x}_{t+1} = A\hat{x}_t + Ke_t$$
$$y_t = C\hat{x}_t + e_t$$

$$(4.1)$$

Where the A-matrix contains the physical information, the C-matrix extracts the information that can be observed by the system response and the K-matrix contains the statistical information. The measured response y_t is generated by two stochastic processes Ke_t and e_t that represent the unmeasured and unknown noise processes.

Three different implementations of the SSI technique are available I ARTeMIS:

-   Unweighted Principal Component (UPC)

-   Principal Component (PC)

-   Canonical Variate Analysis (CVA)

The state space system in Equation 4.1 is estimated by choosing a model order in frequency domain. The choice of model order is crucial since a too low model order will not be able to describe the system and a too high model order will result in an over-specified system, resulting in increased uncertainly of the estimated parameters.

Validation of the time domain estimation of the state space models is performed in frequency domain, which can be visualized in a stabilization diagram. The stabilization diagram shows stable, unstable and noise modes. The criterions for a stable mode are based on deviation in frequency, damping, MAC mode shape and MAC modal amplitude. These criterions can be adjusted to suit the analysed structure. One model order is chosen for each data set. All data sets are the linked together to form the structural modes.

4.1.3   Results of analysis

In the modal analysis of the bridge, nine different measurements were used, denoted Test1 - Test9 in Appendix D. The measurements comprise acceleration response of pedestrian induced vibration. In the analysis five accelerometers were used. In order to estimate the mode shapes some accelerometers were placed in different locations in different measurements. Some of the accelerometers were placed in fixed positions to serve as reference gauges.

Table 4.1 presents the first 10 structural modes identified using the FDD and EFDD techniques. Further classification of the modes is presented in Appendix C. Using the FDD technique results in estimated natural frequencies with a standard deviation σ_f in the range 0.01 Hz – 0.19 Hz corresponding to a relative standard deviation σ_f/f of at most 0.5 %. Corresponding values using the EFDD technique are 0.01 Hz – 0.19 Hz except mode no. 2 that is estimated with a relative standard deviation σ_f/f of 16 %. The damping calculated using EFDD is in the range 0.6 % - 2.5 %. The standard deviation of the damping ratio is more than half the size of the calculated damping ratio, i.e. σ_ξ/ξ is about 50 %.

Table 4.1:   Natural frequencies and estimated damping ratios using FDD and EFDD techniques. Input signal subjected to 15 Hz Low-Pass (LP) filter.

	FDD			Enhanced FDD					
mode no.	f (Hz)	σ_f (Hz)	σ_f/f (%)	f (Hz)	σ_f (Hz)	σ_f/f (%)	ξ (%)	σ_ξ (%)	σ_ξ/ξ (%)
1	1.77	0.009	0.50	1.77	0.009	0.51	1.41	0.799	56.72
2	2.67	0.012	0.46	2.48	0.398	**16.03**	1.28	0.898	69.98
3	2.84	0.011	0.38	2.81	0.044	1.57	0.57	0.354	61.98
4	5.33	0.012	0.22	5.37	0.101	1.89	0.67	0.415	61.89
5	5.59	0.020	0.36	5.61	0.023	0.41	1.09	0.429	39.49
6	7.36	0.017	0.24	7.27	0.186	2.56	2.51	1.837	73.07
7	10.53	0.018	0.17	10.62	0.109	1.03	1.11	0.673	60.59
8	10.80	0.028	0.26	10.76	0.042	0.39	0.66	0.310	47.13
9	12.57	0.051	0.41	12.58	0.020	0.16	1.12	0.359	31.90
10	14.50	0.023	0.16	14.51	0.021	0.14	1.27	0.431	34.04

When using the SSI techniques for modal evaluation, it was found to give more accurate results if the signal is decimated. Furthermore, the signals were analysed in two different ranges, 0 to 10 Hz and 9 to 16.7 Hz corresponding to a decimation of 5 and 3 times respectively. When analysing the results in the range 9 to 16.7 Hz, a high-pass (HP) filter of 9 Hz was applied. In all analyses the number of frequency lines corresponds to approximately $\Delta f = 0.01$ Hz.

Table 4.2:   Natural frequencies and estimated damping ratios using FDD and EFDD techniques. Input signal subjected to 5 times decimation, f_{max} = 10 Hz.

	FDD			Enhanced FDD					
mode no.	f (Hz)	σ_f (Hz)	σ_f/f (%)	f (Hz)	σ_f (Hz)	σ_f/f (%)	ξ (%)	σ_ξ (%)	σ_ξ/ξ (%)
1	1.76	0.007	0.40	1.77	0.009	0.51	1.34	0.838	62.64
2	2.67	0.013	0.50	2.68	0.023	0.86	1.11	0.719	65.10
3	2.85	0.014	0.48	2.85	0.009	0.31	0.61	0.529	87.27
4	5.33	0.015	0.28	5.33	0.009	0.16	0.24	0.282	119.47
5	5.58	0.019	0.35	5.61	0.024	0.42	0.90	0.537	59.71
6	7.36	0.016	0.22	7.35	0.133	1.81	2.12	1.599	75.28

Table 4.3:   Natural frequencies and estimated damping ratios using SSI-UPC technique. Input signal subjected to 5 times decimation, f_{max} = 10 Hz.

	UPC					
mode no.	f (Hz)	σ_f (Hz)	σ_f/f (%)	ξ (%)	σ_ξ (%)	σ_ξ/ξ (%)
1	1.75	0.007	0.37	0.79	0.189	23.82
2	2.68	0.018	0.66	0.80	0.364	45.42
3	2.83	0.022	0.78	0.90	0.525	58.54
4	5.33	0.014	0.27	1.37	0.482	35.11
5	5.60	0.046	0.83	1.74	0.850	48.84
6	7.13	0.069	0.97	3.04	0.986	32.48

Table 4.4:   Natural frequencies and estimated damping ratios using SSI-PC technique. Input signal subjected to 5 times decimation, f_{max} = 10 Hz.

	PC					
mode no.	f (Hz)	σ_f (Hz)	σ_f/f (%)	ξ (%)	σ_ξ (%)	σ_ξ/ξ (%)
1	1.75	0.013	0.76	0.96	0.154	16.03
2	2.68	0.018	0.66	0.75	0.297	39.61
3	2.84	0.016	0.55	0.91	0.367	40.20
4	5.32	0.013	0.25	1.39	0.676	48.78
5	5.62	0.041	0.73	1.57	0.541	34.48
6	7.23	0.015	0.21	2.04	0.894	43.76

Table 4.5:   Natural frequencies and estimated damping ratios using SSI-CVA technique. Input signal subjected to 5 times decimation, f_{max} = 10 Hz.

	CVA					
mode no.	f (Hz)	σ_f (Hz)	σ_f/f (%)	ξ (%)	σ_ξ (%)	σ_ξ/ξ (%)
1	1.75	0.014	0.80	1.21	0.649	53.66
2	2.68	0.018	0.66	1.01	0.693	68.58
3	2.84	0.016	0.58	1.05	0.688	65.76
4	5.32	0.017	0.31	1.21	0.262	21.67
5	5.62	0.057	1.02	1.26	0.458	36.41
6	7.34	0.070	0.95	1.69	0.535	31.60

Table 4.6:   Natural frequencies and estimated damping ratios using FDD and EFDD tech-
niques. Input signal subjected to 3 times decimation, f_{max} = 16.7 Hz and a HP-filter
up to 9 Hz.

	FDD			Enhanced FDD					
mode no.	f (Hz)	σ_f (Hz)	σ_f/f (%)	f (Hz)	σ_f (Hz)	σ_f/f (%)	ξ (%)	σ_ξ (%)	σ_ξ/ξ (%)
7	10.54	0.018	0.17	10.61	0.095	0.89	1.00	0.552	55.31
8	10.81	0.025	0.23	10.78	0.046	0.43	0.58	0.331	56.95
9	12.57	0.052	0.41	12.58	0.019	0.15	0.96	0.313	32.73
10	14.47	0.033	0.23	14.40	0.030	0.21	1.08	0.145	13.40

Table 4.7:   Natural frequencies and estimated damping ratios using SSI-UPC technique. Input
signal subjected to 3 times decimation, f_{max} = 16.7 Hz and a HP-filter up to 9 Hz.

	UPC					
mode no.	f (Hz)	σ_f (Hz)	σ_f/f (%)	ξ (%)	σ_ξ (%)	σ_ξ/ξ (%)
7	10.57	0.049	0.47	1.51	1.005	66.42
8	10.80	0.032	0.30	1.32	1.180	89.39
9	12.56	0.025	0.20	0.99	0.223	22.54
10	14.47	0.030	0.21	1.37	0.320	23.27

Table 4.8:   Natural frequencies and estimated damping ratios using SSI-PC technique. Input
signal subjected to 3 times decimation, f_{max} = 16.7 Hz and a HP-filter up to 9 Hz.

	PC					
mode no.	f (Hz)	σ_f (Hz)	σ_f/f (%)	ξ (%)	σ_ξ (%)	σ_ξ/ξ (%)
7	10.55	0.082	0.78	1.06	0.534	50.57
8	10.80	0.029	0.27	1.33	0.900	67.74
9	12.58	0.019	0.15	1.01	0.273	26.90
10	14.49	0.036	0.25	1.27	0.264	20.88

Table 4.9:   Natural frequencies and estimated damping ratios using SSI-PC technique. Input
signal subjected to 3 times decimation, f_{max} = 16.7 Hz and a HP-filter up to 9 Hz.

	CVA					
mode no.	f (Hz)	σ_f (Hz)	σ_f/f (%)	ξ (%)	σ_ξ (%)	σ_ξ/ξ (%)
7	10.60	0.076	0.72	1.36	0.536	39.26
8	10.84	0.035	0.32	2.34	1.786	76.19
9	12.56	0.019	0.15	1.06	0.307	29.08
10	14.48	0.057	0.39	1.39	0.640	46.17

The result in Table 4.1 – Table 4.9 shows good agreement in both estimated frequency and
damping ratio between the different analysis methods. The natural frequencies are in most cases
estimated within 1 %. The damping ratio is estimated to approximately 1 % both using the
EFDD and the different SSI-methods. The standard deviation of the damping ratio are on the
other hand rather large, expressed as σ_ξ/ξ approximately 15 – 120 % for the EFDD method and
20 – 80 % for the SSI methods.

4.2   Signal processing using Matlab

Some signal processing has been performed using Matlab, primary to confirm the damping ratio from the lowest mode. Field measurement denoted Test12 comprised a transient excitation of one 100 kg person at bridge mid-span. The vertical acceleration, presented in Figure C.12 has been studied. Since each natural frequency has a unique damping ratio the modes must be separated in order to estimate the damping for a single frequency. Figure 4.1 shows the difference in response between an unfiltered signal and a separation of the first natural frequency. During the transient excitation, mainly the two first modes were excited, corresponding to the first antimetric and first symmetric vertical bending modes respectively. The peak to peak acceleration is 0.14 m/s^2 for both modes which of the first contributes to 0.06 m/s^2. This is also seen in the frequency response in Figure 4.2. Since the modes are close to each other, a steep filter design is needed to attenuate the second mode. Figure 4.2 shows that a 8th order Butterworth filter is not able to attenuate the second mode sufficiently. Using an 8th order Elliptic filter on the other hand, results in almost complete attenuation of the second mode without altering the first mode.
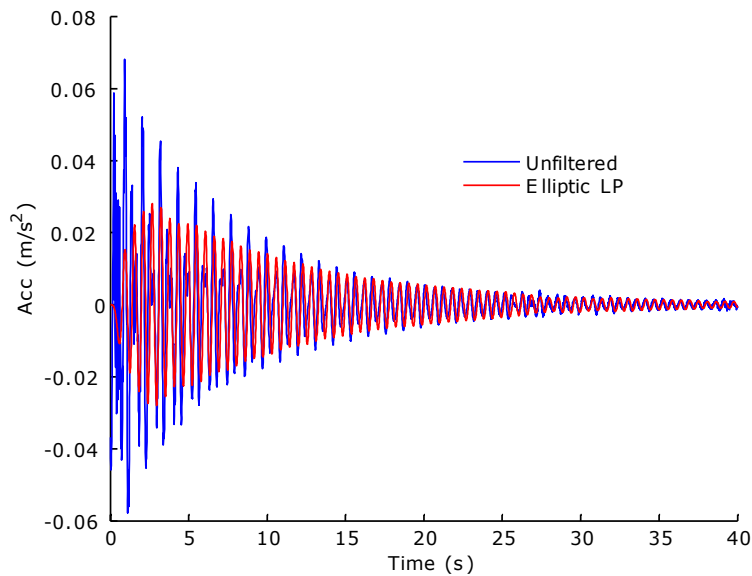
Figure 4.1:   Damped vibration for unfiltered and filtered signal, transient excitation.
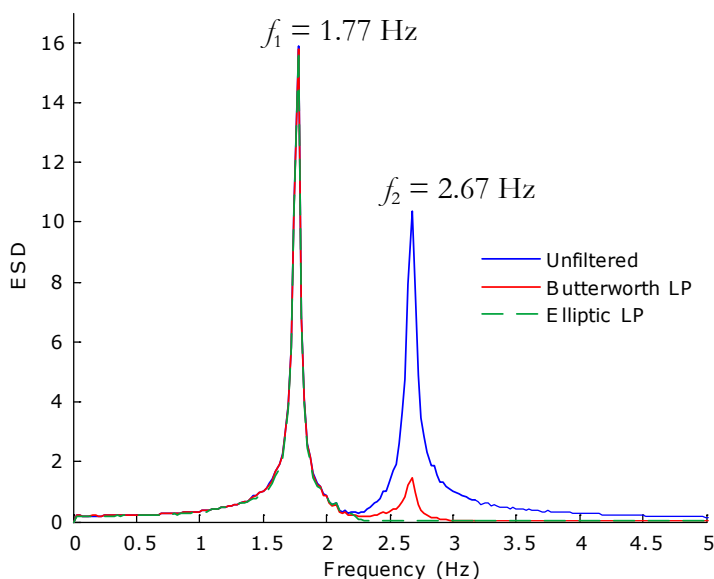
Figure 4.2:   Frequency domain respones of the transient signal.

17

The damping ratio has been estimated for the first mode using two different techniques, decay of motion in time domain and band-width method in frequency domain. The curve-fitting in time-domain is shown in Figure 4.3, resulting in an estimated damping $\xi = 0.85$ %. The estimation using the band-width method in frequency domain is shown in Figure3 4.4 resulting in an estimated damping ratio $\xi = 0.95$ %. The results from the modal analysis in ARTeMIS are presented in Table 4.10.
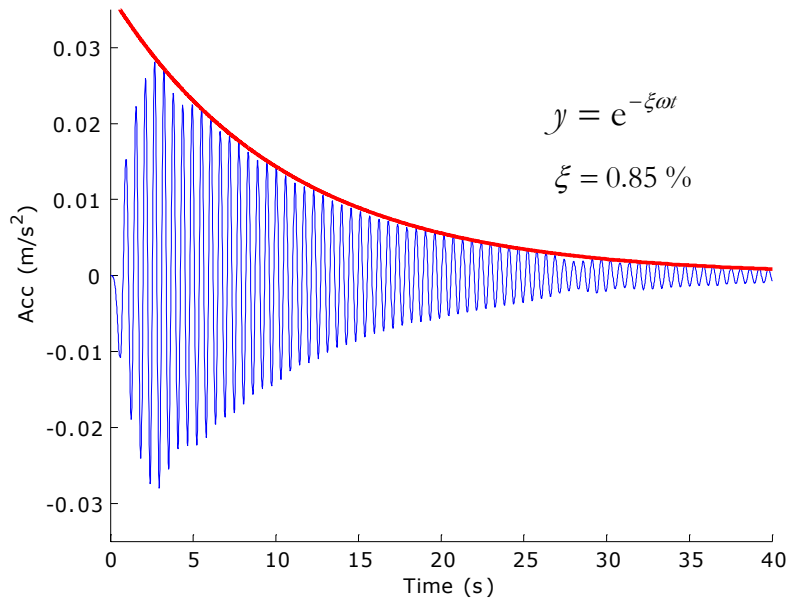
Figure 4.3:   Curve fitting of decay of motion in time domain.
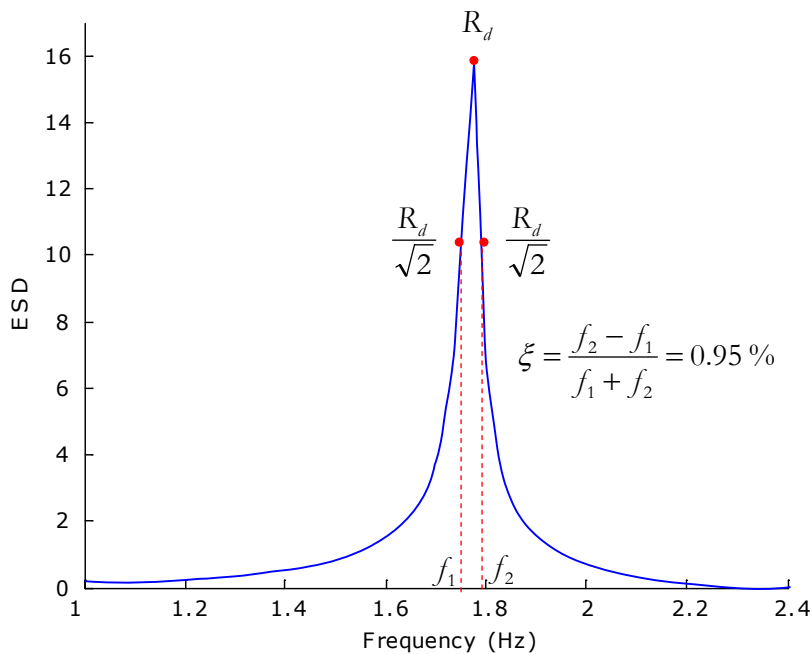
Figure 4.4:   Estimating the damping in frequency domain using the band-width method.

Table 4.10:   Estimations of the first natural frequency and damping ratio using EFDD and all
SSI methods, based on abient vibrations in field measurements Test1 – Test9.

Method:	f (Hz)	σ_f (Hz)	σ_f/f (%)	ξ (%)	σ_ξ (%)	σ_ξ/ξ (%)
EFDD	1.77	0.009	0.51	1.34	0.838	62.64
SSI-UPC	1.75	0.007	0.37	0.79	0.189	23.82
SSI-PC	1.75	0.013	0.76	0.96	0.154	16.03
SSI-CVA	1.75	0.014	0.80	1.21	0.649	53.66

The estimation of the damping presented in Table 4.10 shows rather good agreement with the analysis of the transient signal. Variation in damping ratio may also differ depending on the load, partly due to different amplitude from the ambient pedestrian load compared to the transient excitation of a single person, but partly due to interaction between the bridge and the pedestrians. In both cases the damping should increase. The damping ratio can roughly be estimated to 1 %.

19

5 Conclusions

When comparing the results from the FE-model with the modal analysis based on the measured response, it was found that the bearing friction had large influence on the results, mainly considering the natural frequency. The degree of restraint in the column was also found to be of great importance. The column is founded on a group of piles resulting in a significant elastic restraint rather that fully clamped.

When identifying the static manner of action the bridge is subjected to, the mode shapes estimated from the modal analysis played a significant role. For reasonable proper boundary conditions in the FE-analysis the same mode shape could be identified from both modal analysis and FE-analysis. The influence of the parameters in the FE-model could then be evaluated to correspond to the modal analysis regarding natural frequency. The FE-analysis also provided information where physical modes should appear in the modal analysis. The first 10 structural modes, involving vertical, transversal and torsion modes were found and paired between the FE-analysis and the modal analysis.

The natural frequencies contained in the measured signals were found to be estimated within 0.5 – 1.0%. The estimation of the damping ratio on the other hand, involved large uncertainties although the average damping ratio was found at about 1 %. This was also confirmed from analysis of transient excitation. In the case of transient excitation, the damping ratio was evaluated using the decay of a single frequency.

As the lowest natural frequencies were obtained under 3.5 Hz, acceleration analysis must be performed for these frequencies according the Swedish Road Regulations, Bro 2004. The analysis was performed by the bridge constructor and showed allowable values using the damping ratio 0.6 %. Using the estimated damping 1 % increase the safety of acceleration criteria. Although the damping ratio was found to be higher than in the design codes and that the acceleration criterion was fulfilled, clearly noticeable vibration was noticed. The bridge could be set in motion by only a few pedestrian, using simultaneous walking. In the last field measurement, denoted Test13, four pedestrians was able to produce a peak to peak acceleration of 0.4 m/s^2 by synchronized walking. This can be compared to a peak to peak acceleration of 0.3 m/s^2 from 16 pedestrians walking unsynchronized, as in measurement Test1 to Test9. The reason why the bridge easily can be set in motion is due to the slender construction with low mass, in combination with a resonance frequency near normal walking pace.

Bibliography

1/ Blanco C.M., Bouillard Ph., Bodarwé E., Ney L. Structural dynamic design of a footbridge under pedestrian loading. *9ᵗʰ SAMTECH Users Conference 2005.*

2/ Fitzpatrick T., Dallard P., Le Bourva S., Low A., Ridsdill Smith R., Willford M. Linking London: The Millenium Bridge. *The Academy of Engineering, 29 Great Peter Street, Westminister, London SW1P 3LW, ISBN 1 871634 99 7, June 2001.*

3/ Nakamura S., Kawasaki T. Lateral vibration of footbridges by synchronous walking. *Journal of Constructional Steel Research (2006), doi:10.1016/j.jcsr.2006.06.023.*

4/ Newland D.E. Pedestrian Excitation of Bridges – Recent Results. *Tenth International Congress on Sound and Vibration, Stockholm Sweden 7-10 July 2003.*

5/ Obata T., Miyamori Y. Identification of a human walking force model based on dynamic monitoring data from pedestrian bridges. *Computers & Structures 84 (2006) 541-548.*

6/ Ronnebrant R., Rosell E. Vägverkets allmänna tekniska beskrivning för nybyggande och förbättring av broar Bro 2004. *Publikation 2004:56 ISSN 1401-9612.*

7/ Živanović S., Pavic A., Reynolds P. Modal testing and FE model tuning of a lively footbridge structure. *Engineering Structures 28 (2006) 857-868.*

8/ Živanović S., Pavic A., Reynolds P. Vibration serviceability of footbridges under human-induced excitation: a literature review. *Journal of Sound and Vibration 279 (2005) 1-74.*

9/ Zoltowski K., Zoltowski P. Dynamic analysis of pedestrian bridges with FEM and CFD. *Gdansk University of Technology, KBP Zoltowski (Consulting Engineers), Gdansk.*

A   General assembly drawings
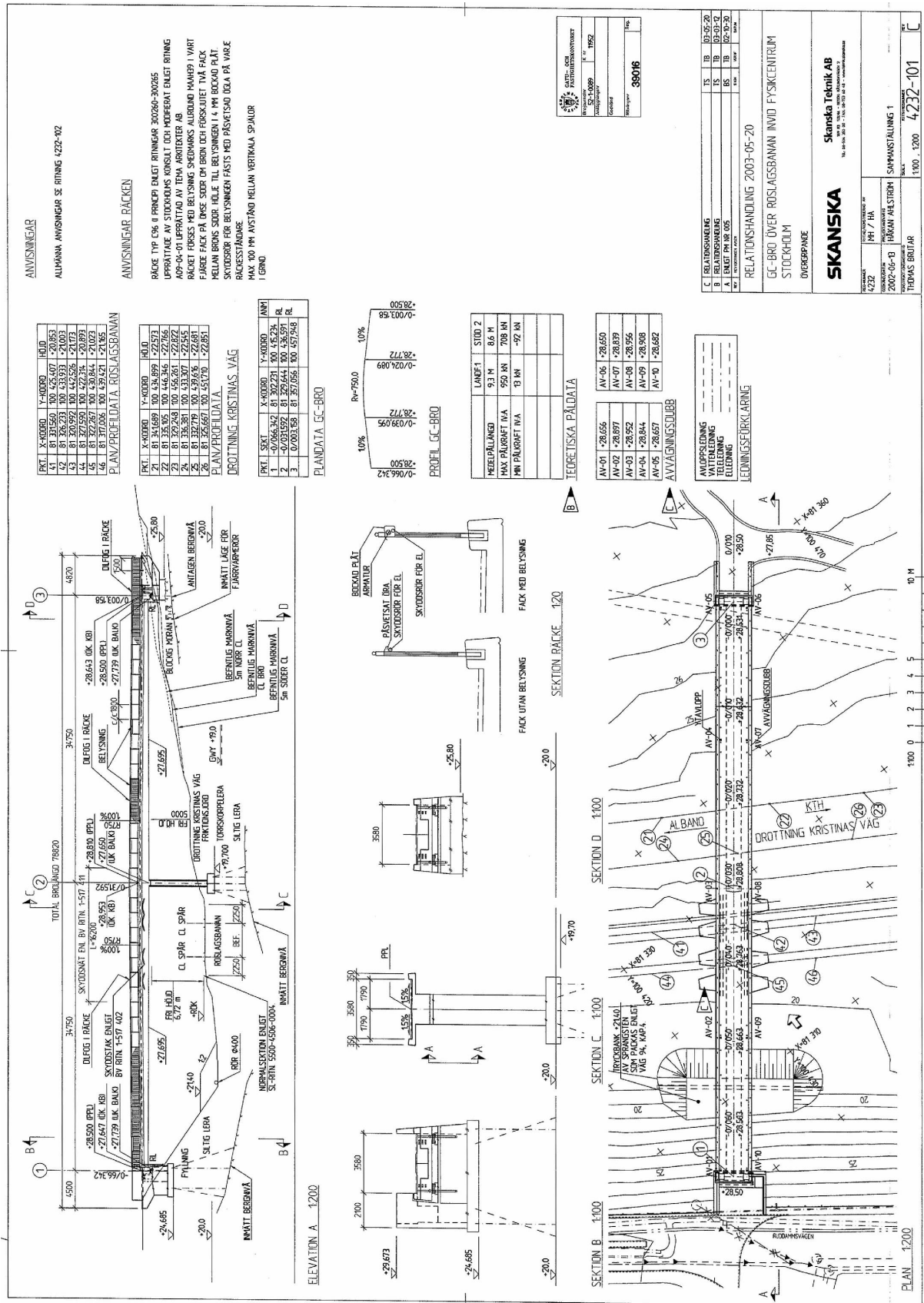
Figure A.1:   General assemby drawing of the bridge.

Figure A.2:   Group of piles.

Figure A.3:   Bearings.
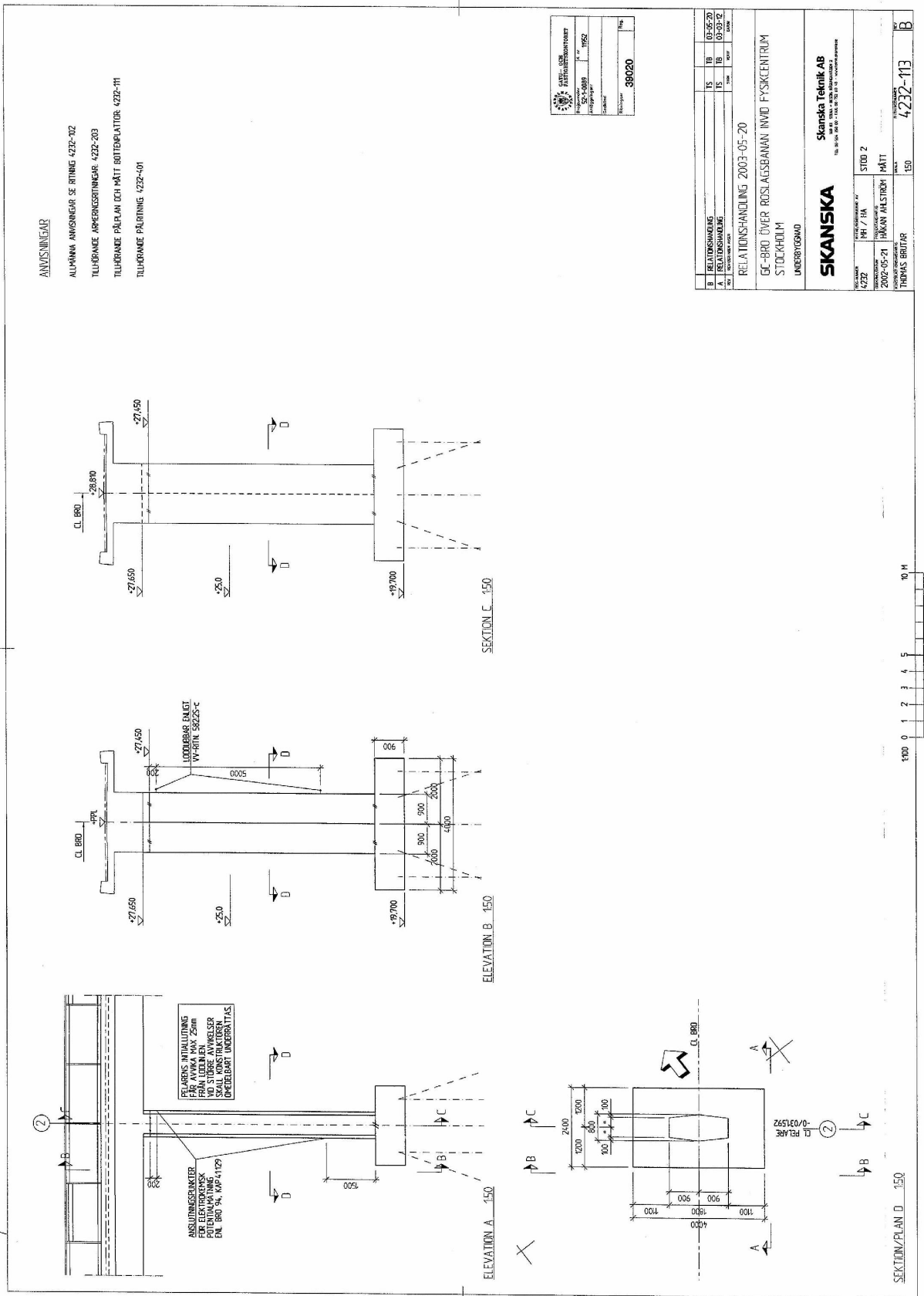
Figure A.4:   Column.
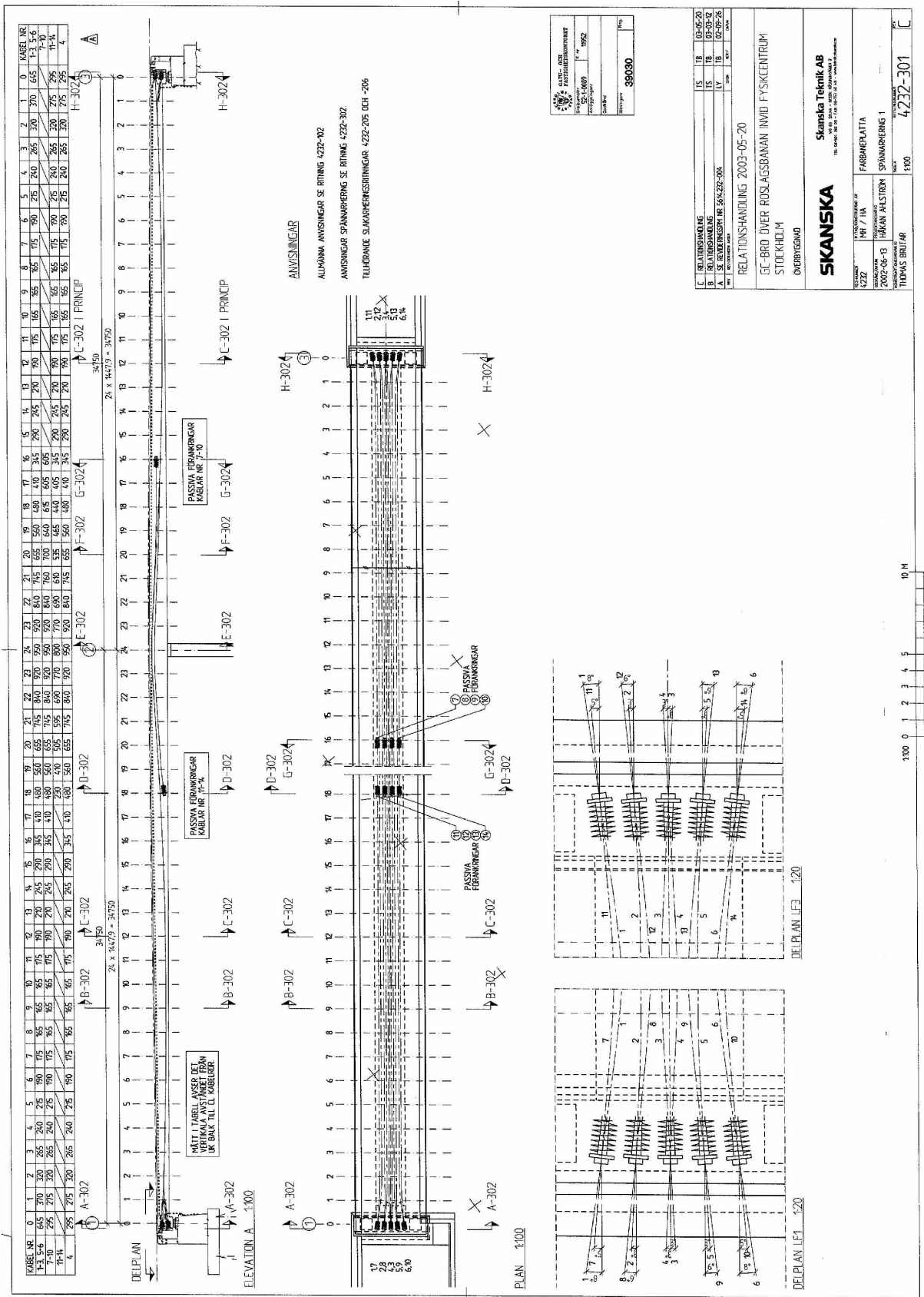
Figure A.5:   Post tendons.

B   Schedule of performed measurements

The following appendix includes a schedule of the field measurements performed at the bridge the 5th of October 2006.

Instrumentation

The instrumentation comprises gauges presented in Table B.1. The assembly of the gauges on the bridge are presented in Figure B.1. Gauges in channel 2, 4, 5, 7, 8, 9, 10 are placed in fix positions along the line N12 – S12. The gauge in channel 3 is placed in different positions N1 to N6 and gauge in channel 6 is placed in different positions S1 to S6. When the gauges are mounted on the column, gauge in channel 3 is oriented transversally in P1 and gauge in channel 6 longitudinally in P1. The point P1 is defined at 1 m from the top of the column and in the centre transversally. When mounted at the column, gauge in channel 3 is defined positive at north and gauge in channel 6 positive at east. The data is collected with a sample rate 100 Hz and using a Bessel LP-filter at 20 Hz to avoid aliasing.

Table B.1:   Gauge positioning and structure of measurement channels.

Channel:	Gauge type:	Transversal position	Direction:
1	Time		
2	LVDT, KTH	Centre, fix	vertical
3	Acc, KTH	north, movable	vertical, (transversal on column)
4	Acc, KTH	north, fix (N12)	transversal, positive at south
5	Acc, KTH	north, fix (N12)	vertical
6	Acc, KTH	south, movable	vertical, (longitudinal at column)
7	Acc, KTH	south, fix (S12)	vertical
8	Laser, LTU	north, fix	vertical, positive uppwards
9	Laser, LTU	north, fix	transversal, positive at south
10	Acc, LTU	north, fix (N12)	vertical
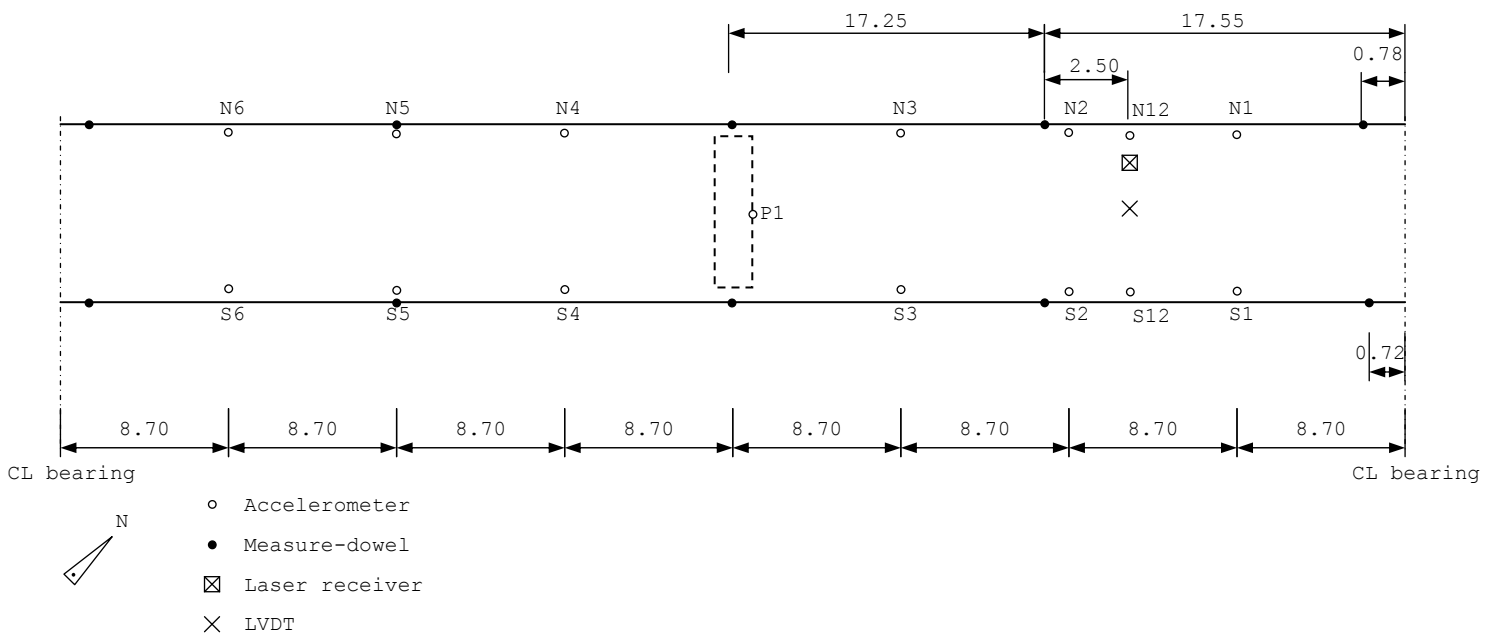
Figure B.1:   Instrumentation assembly and location of measure-dowels.

31

Performed measurements

The measurements were performed according to Table B.2. During measurement denoted Test1 to Test9 the gauge in channel 10 measures vertical acceleration. During measurement denoted Test10 to Test13 this gauge measures vertical displacement. During Test9 to Test13 the gauges in channel 3 and 6 are placed at the column.

Table B.2: Field measurement schedule.

	Gauge position			
File name:	**gauge 3:**	**gauge 6:**	**Start time:**	**Note:**
Test1	N1	S1	11:15	Random pedestrian excitation
Test2	N2	S2	11:30	Random pedestrian excitation
Test3	N2, transv.	S5	11:50	Random pedestrian excitation
Test4	N3	S3	12:01	Random pedestrian excitation
Test5	N4	S4	12:12	Random pedestrian excitation
Test6	N5	S5	12:24	Random pedestrian excitation
Test7	N5, transv.	S2	12:45	Random pedestrian excitation
Test8	N6	S6	13:00	Random pedestrian excitation
Test9	P1, transv.	P1, long.	13:40	Random pedestrian excitation
Test10	P1, transv.	P1, long.	13:50	Longitudinally excitation, jumping pedestrians in the west span, adjusted gauge factors for channel 9 that now measures vertical displacement
Test11	P1, transv.	P1, long.	14:00	Synchronized pedestrian excitation, 10 persons: - walks along the bridge from east to west - jumps in the west mid-span - jumps on each side of the bridge transversally - everyone is jumping at the south side
Test12	P1, transv.	P1, long.	14:10	Excitation using known mass: One person (100 kg) is jumping two times in the west mid-span. Walks to the east mid-span and jumps two times.
Test13	P1, transv.	P1, long.	14:15	Synchronized pedestrian excitation, 4 persons. Walking side by side from east to west, then back again. No other pedestrians at the bridge.

C   Assembly of measured signals
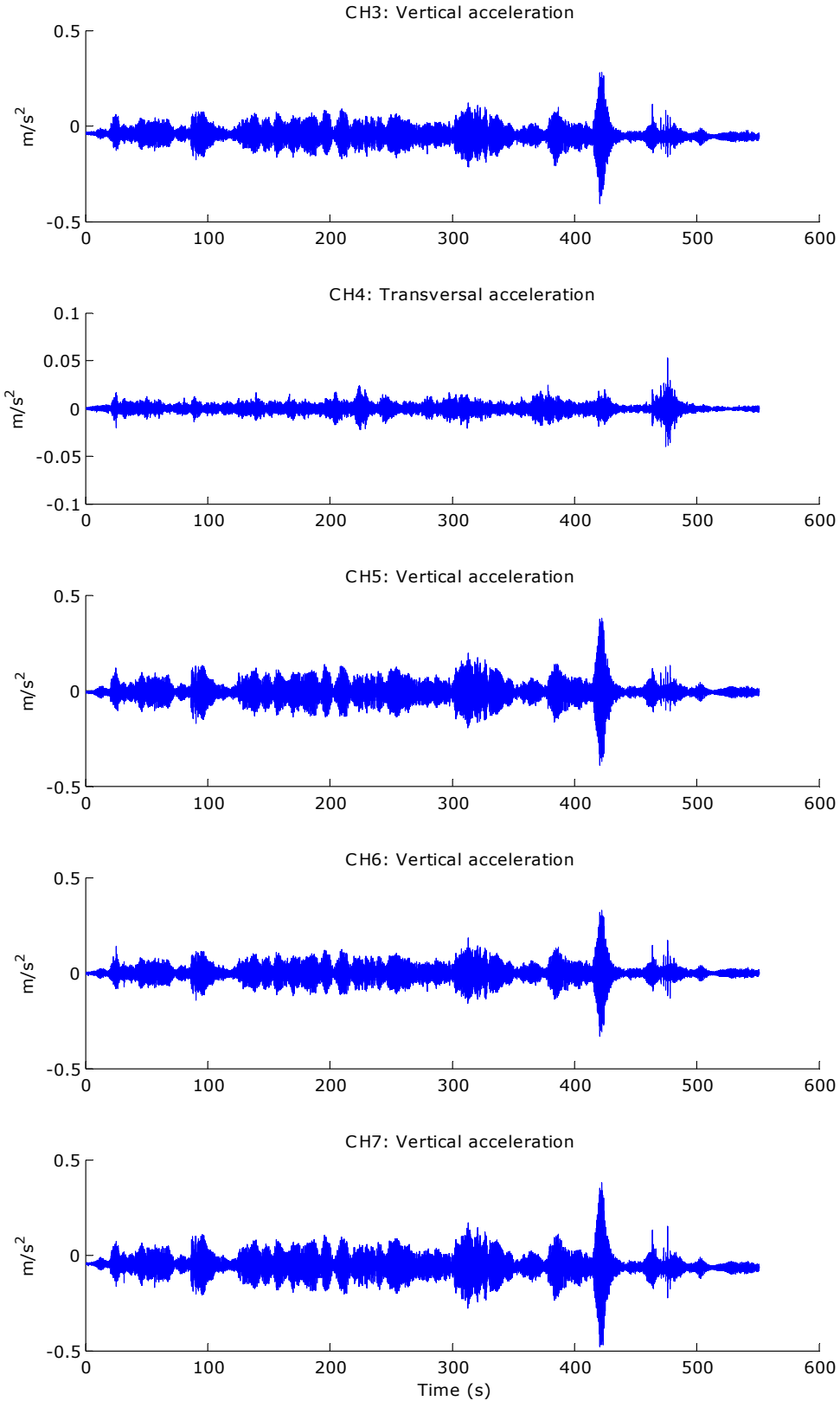
Figure C.1:   Field measurement no. 1, presentation of accelerometer signals used in modal analysis.
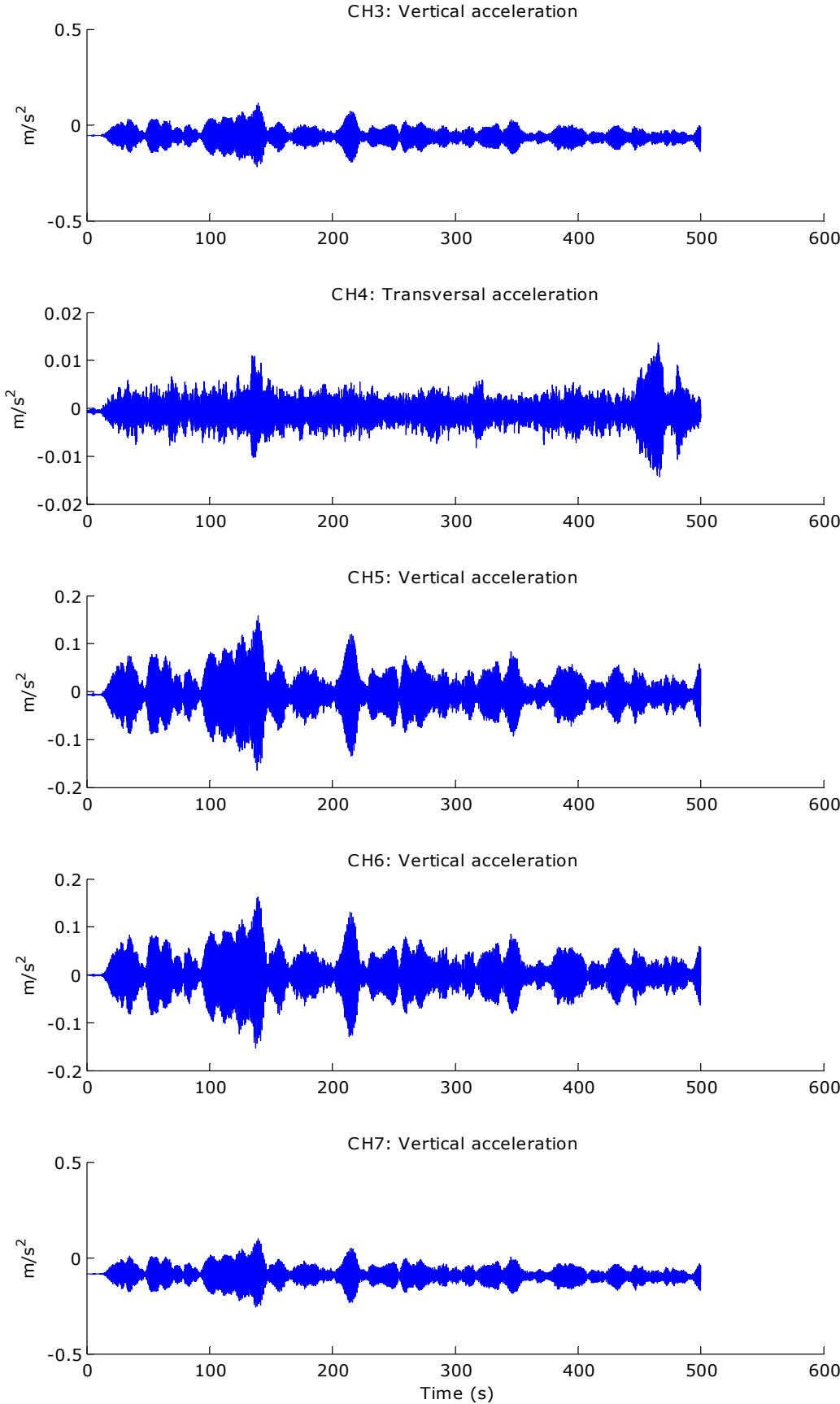
Figure C.2: Field measurement no. 2, presentation of accelerometer signals used in modal analysis.
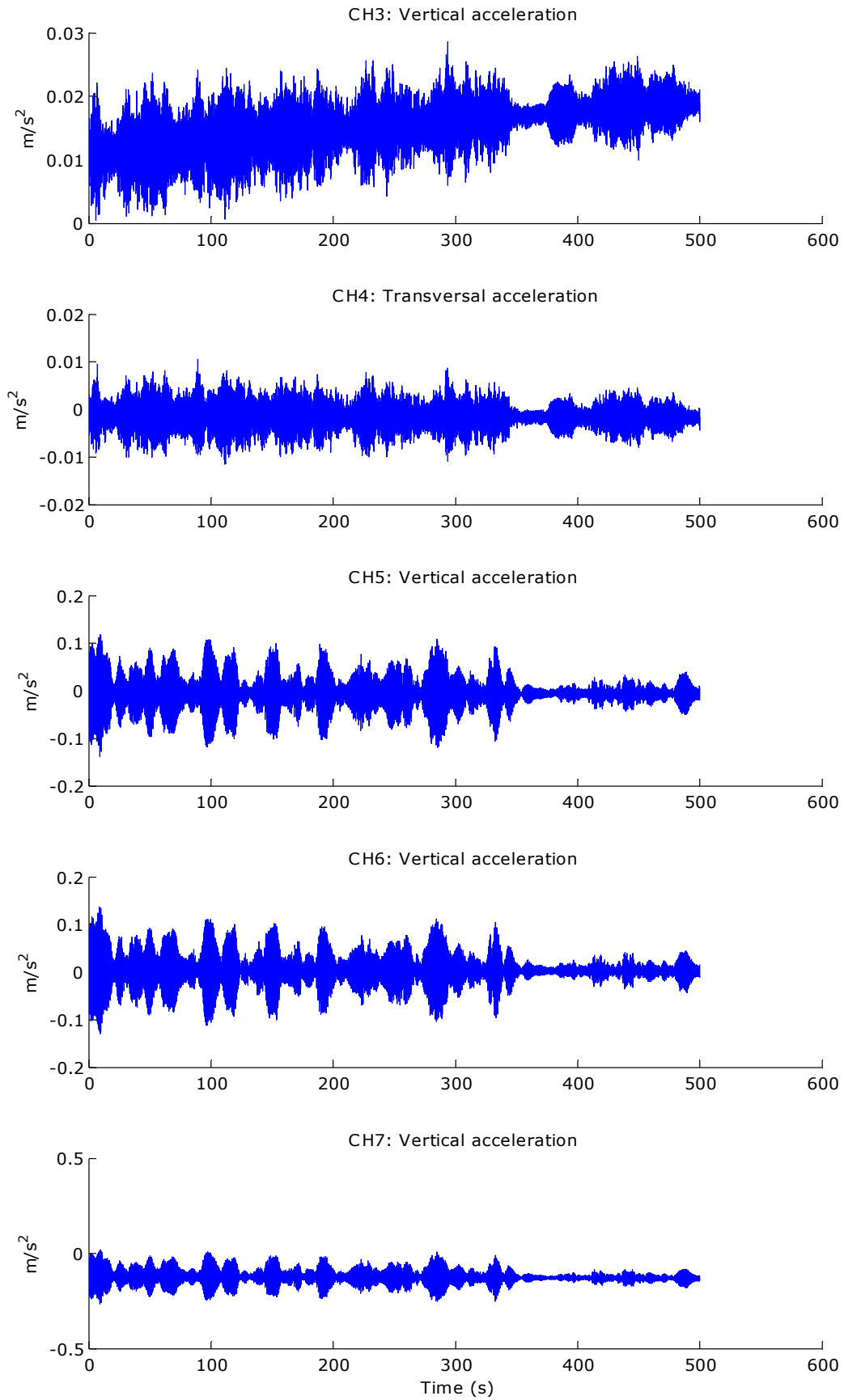
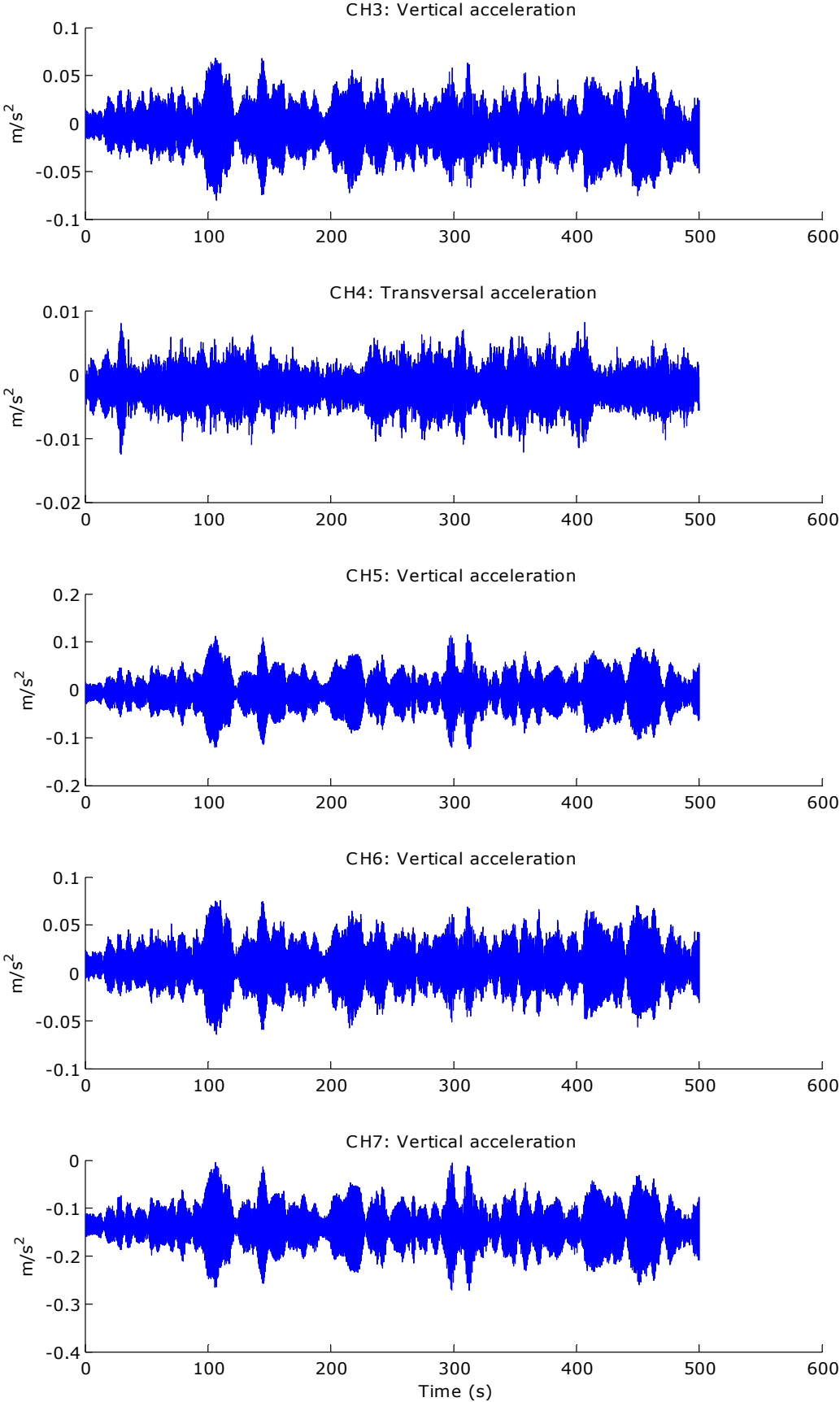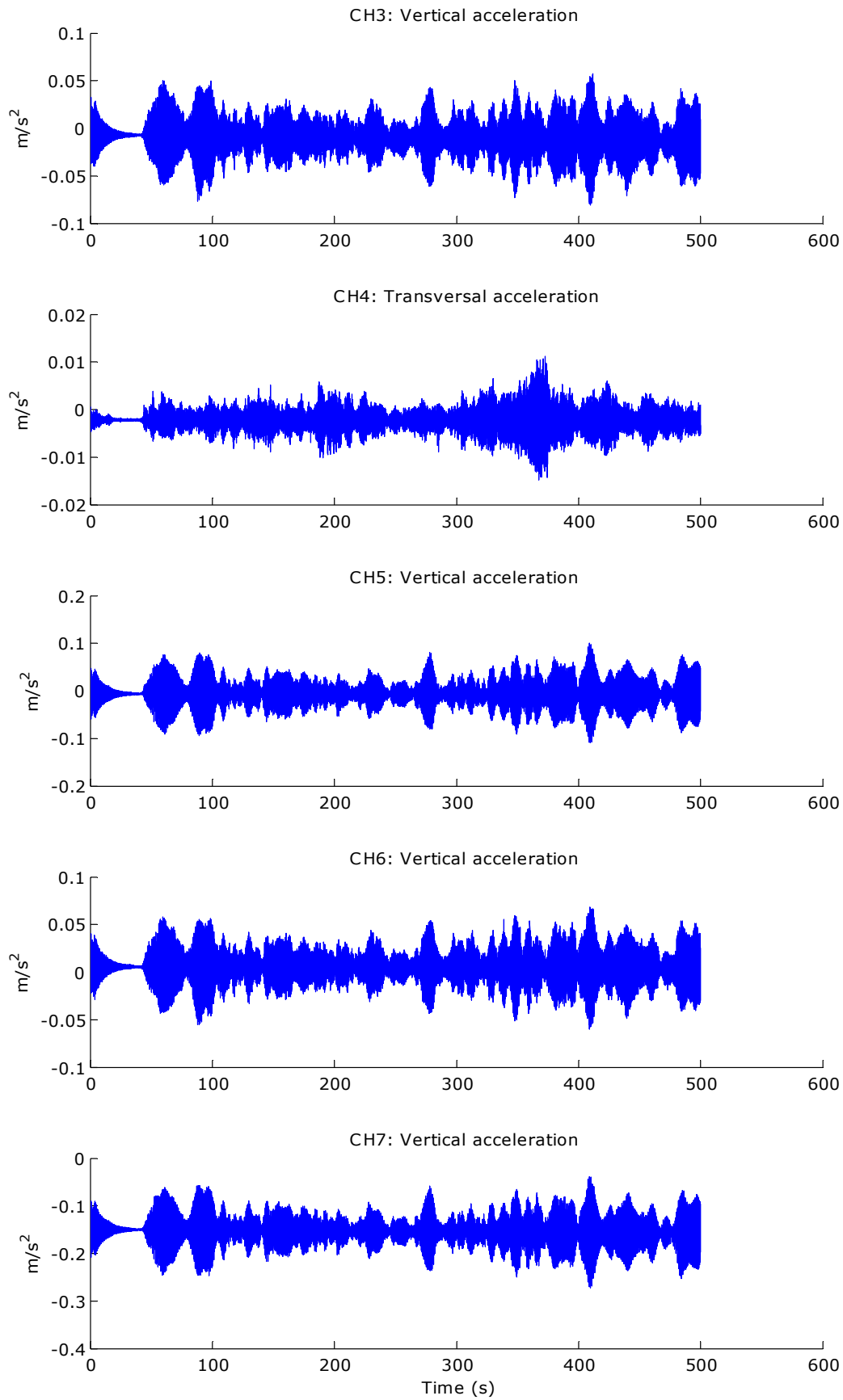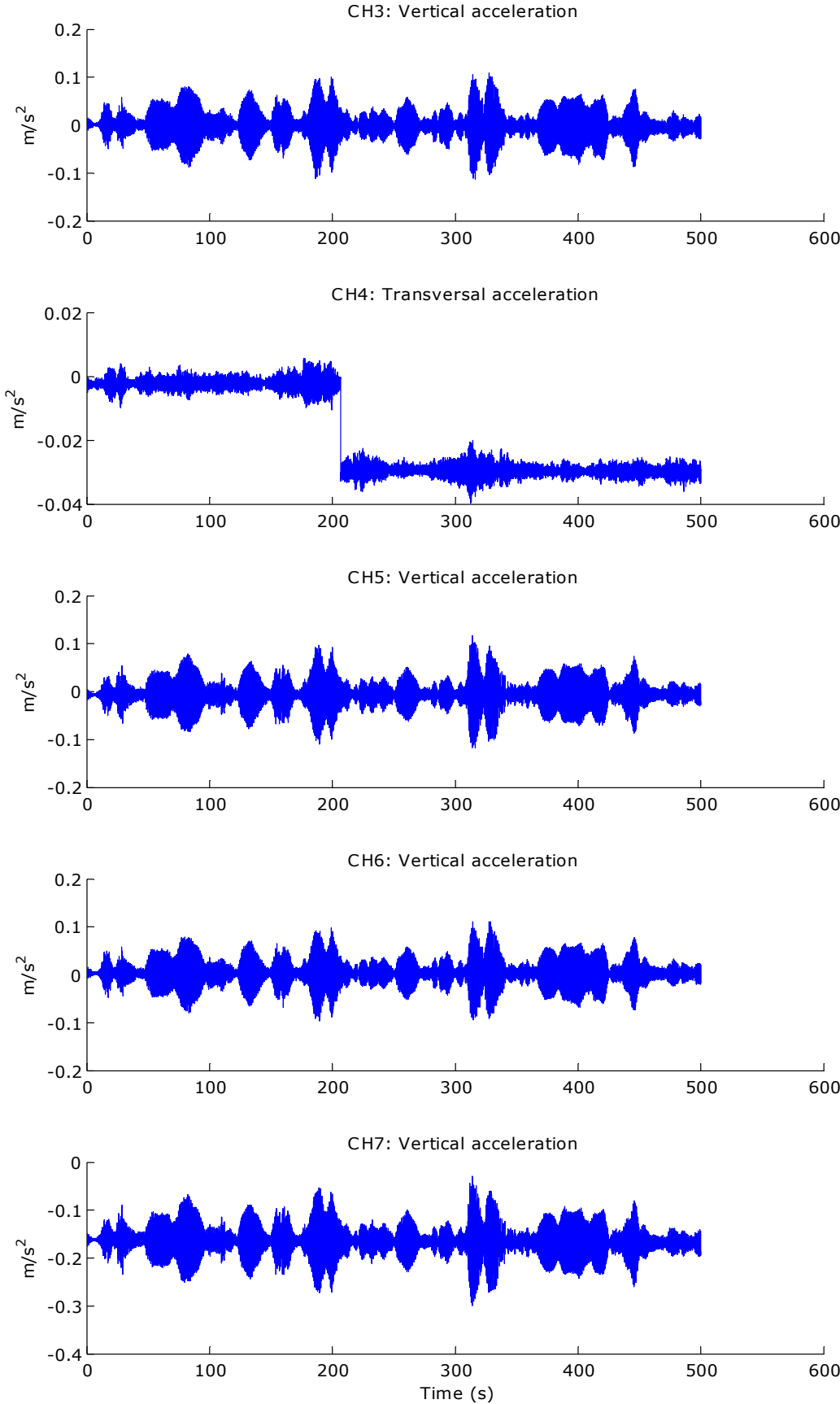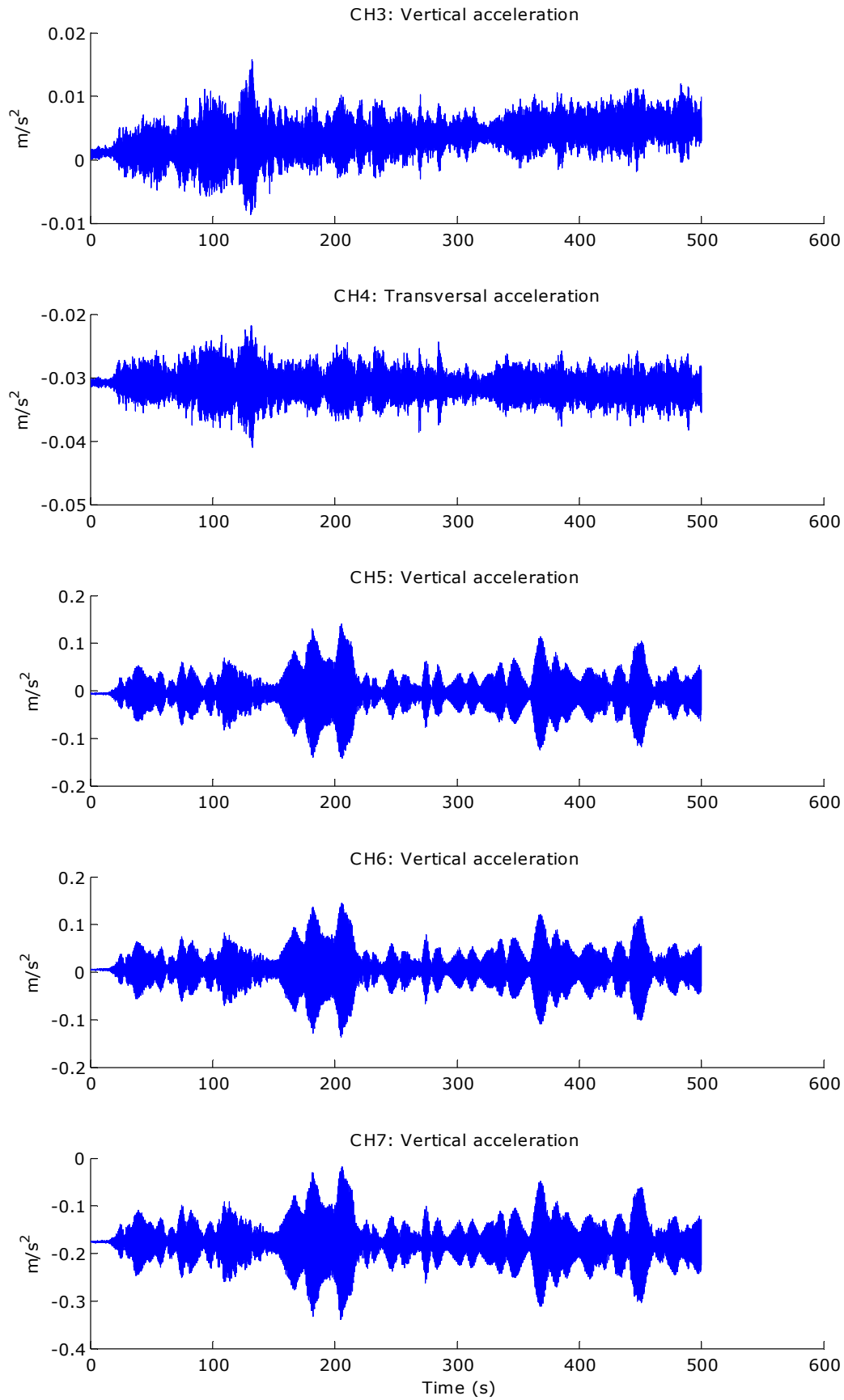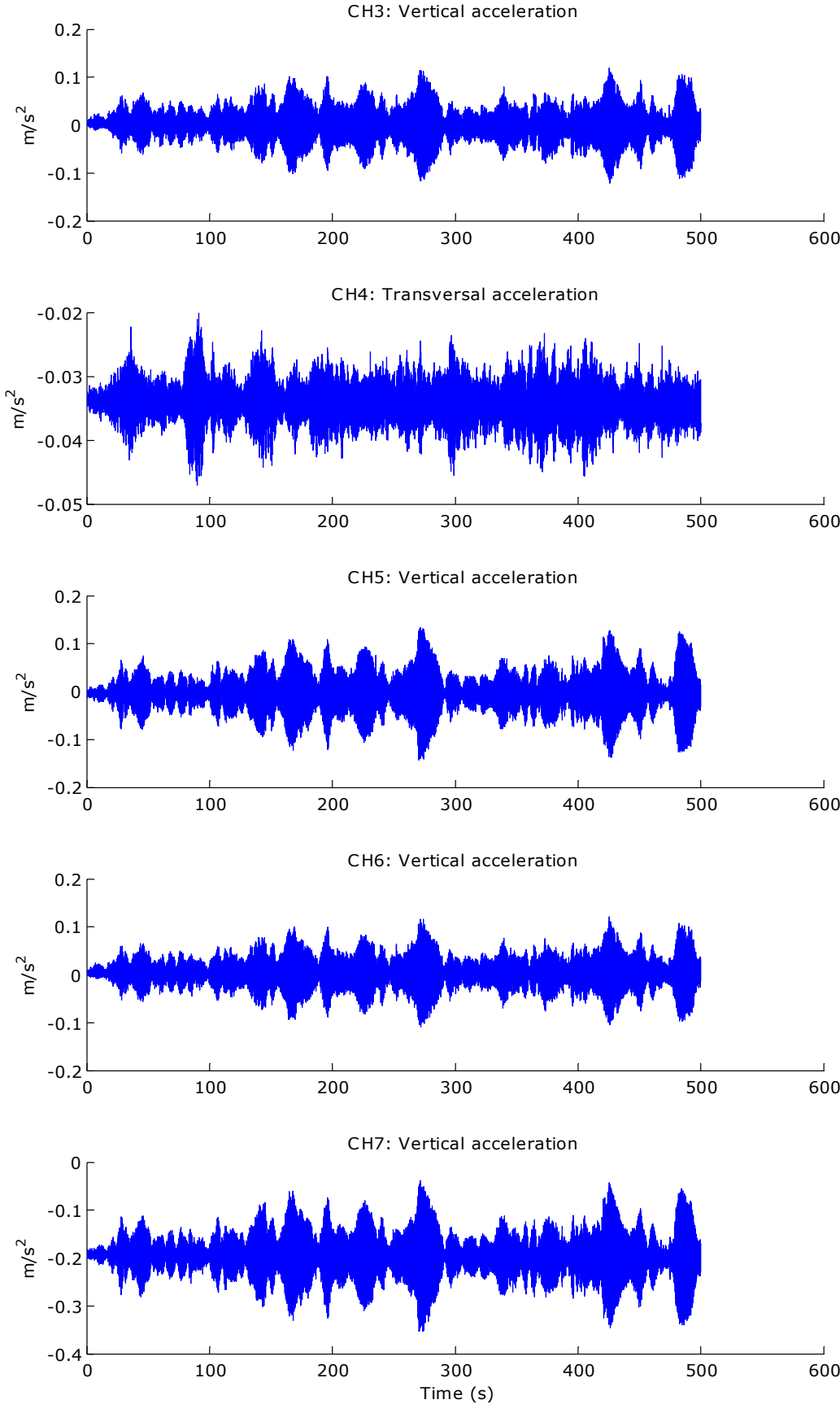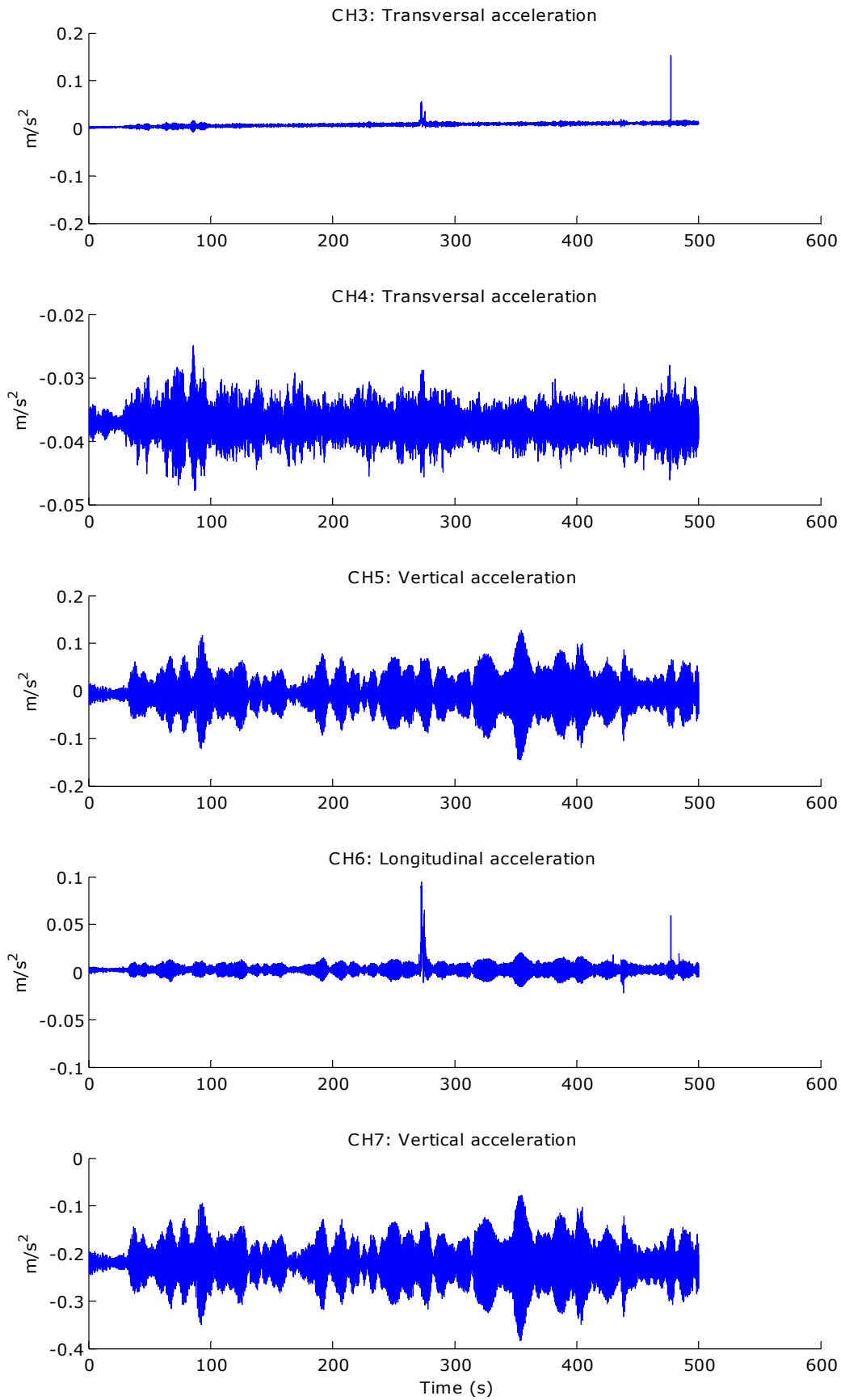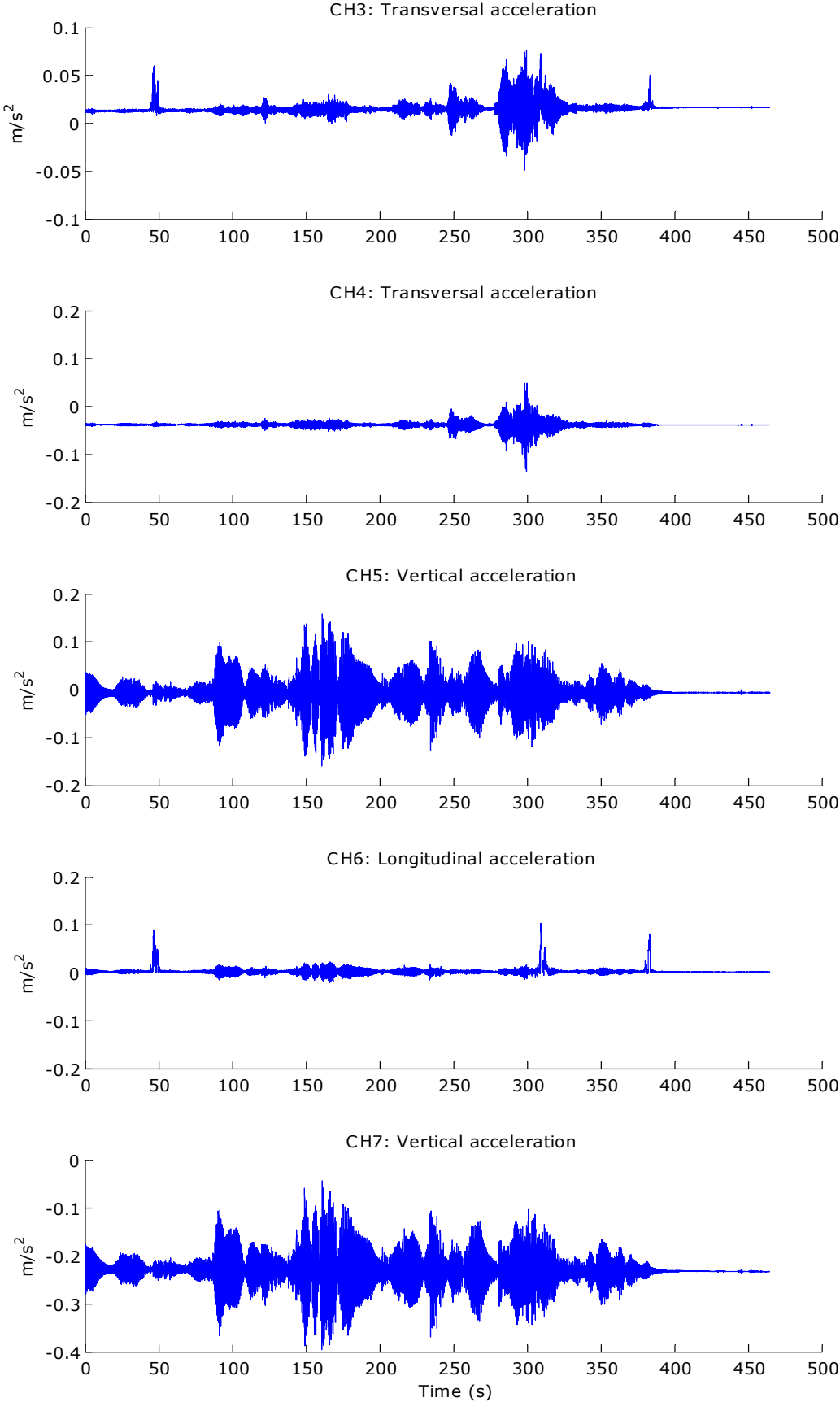Figure C.3: Field measurement no. 3, presentation of accelerometer signals used in modal analysis.

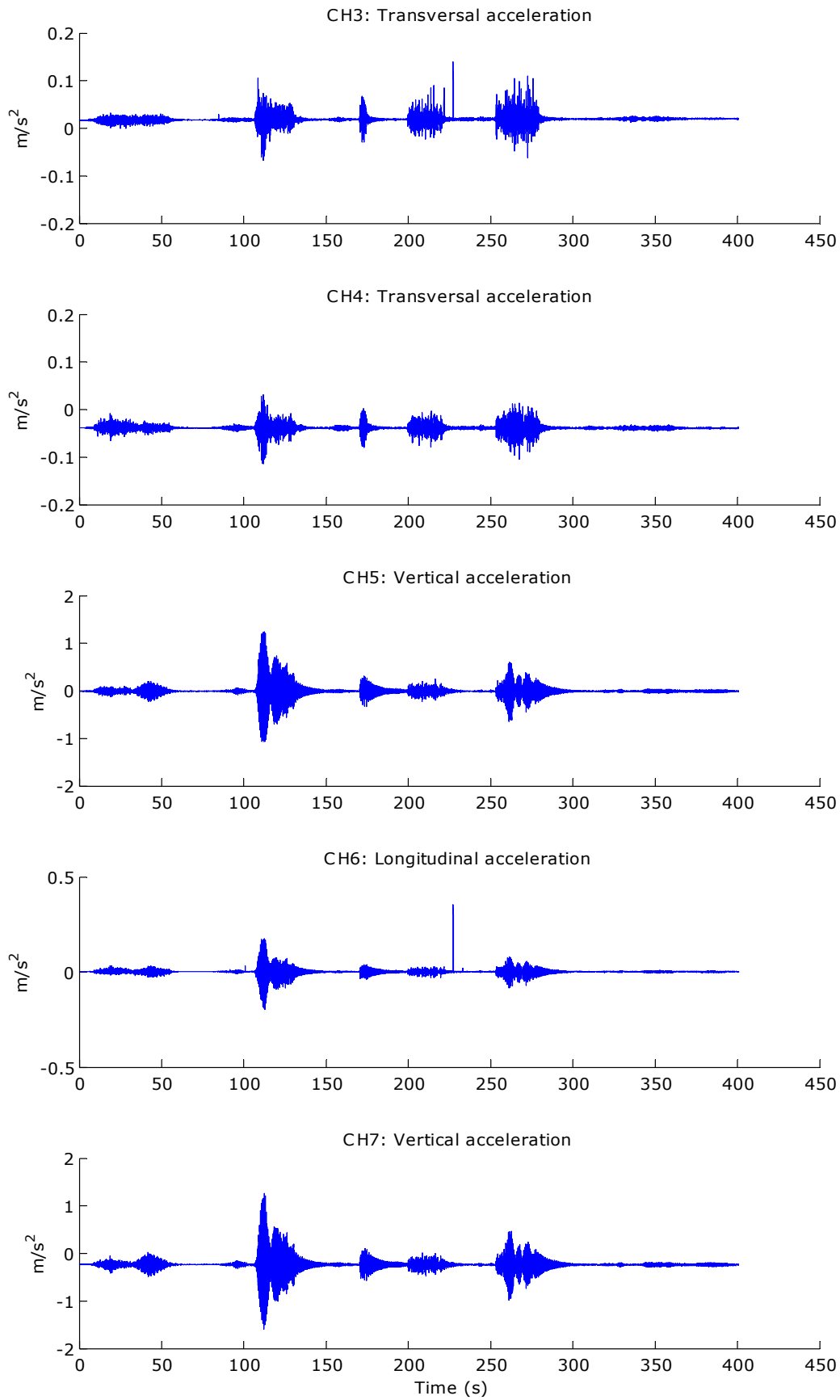Figure C.4: Field measurement no. 4, presentation of accelerometer signals used in modal analysis.

Figure C.5: Field measurement no. 5, presentation of accelerometer signals used in modal analysis.

Figure C.6: Field measurement no. 6, presentation of accelerometer signals used in modal analysis.

Figure C.7:   Field measurement no. 7, presentation of accelerometer signals used in modal analysis.

Figure C.8:   Field measurement no. 8, presentation of accelerometer signals used in modal analysis.

Figure C.9: Field measurement no. 9, presentation of accelerometer signals used in modal analysis.

Figure C.10: Field measurement no. 10, presentation of accelerometer signals from forced excitation of the bridge.

Figure C.11: Field measurement no. 11, presentation of accelerometer signals from forced excitation of the bridge.
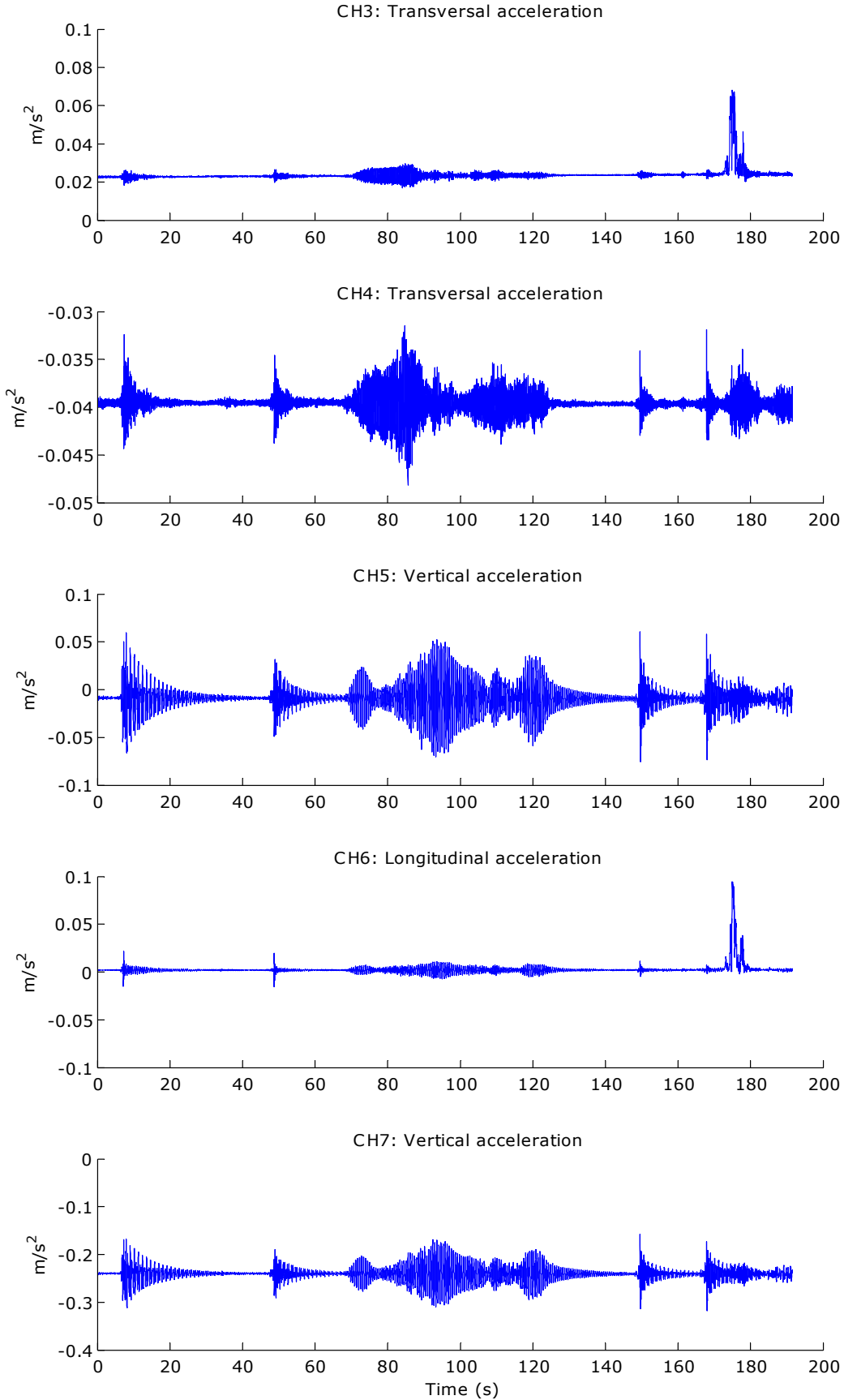
Figure C.12: Field measurement no. 12, presentation of accelerometer signals from forced excitation of the bridge.
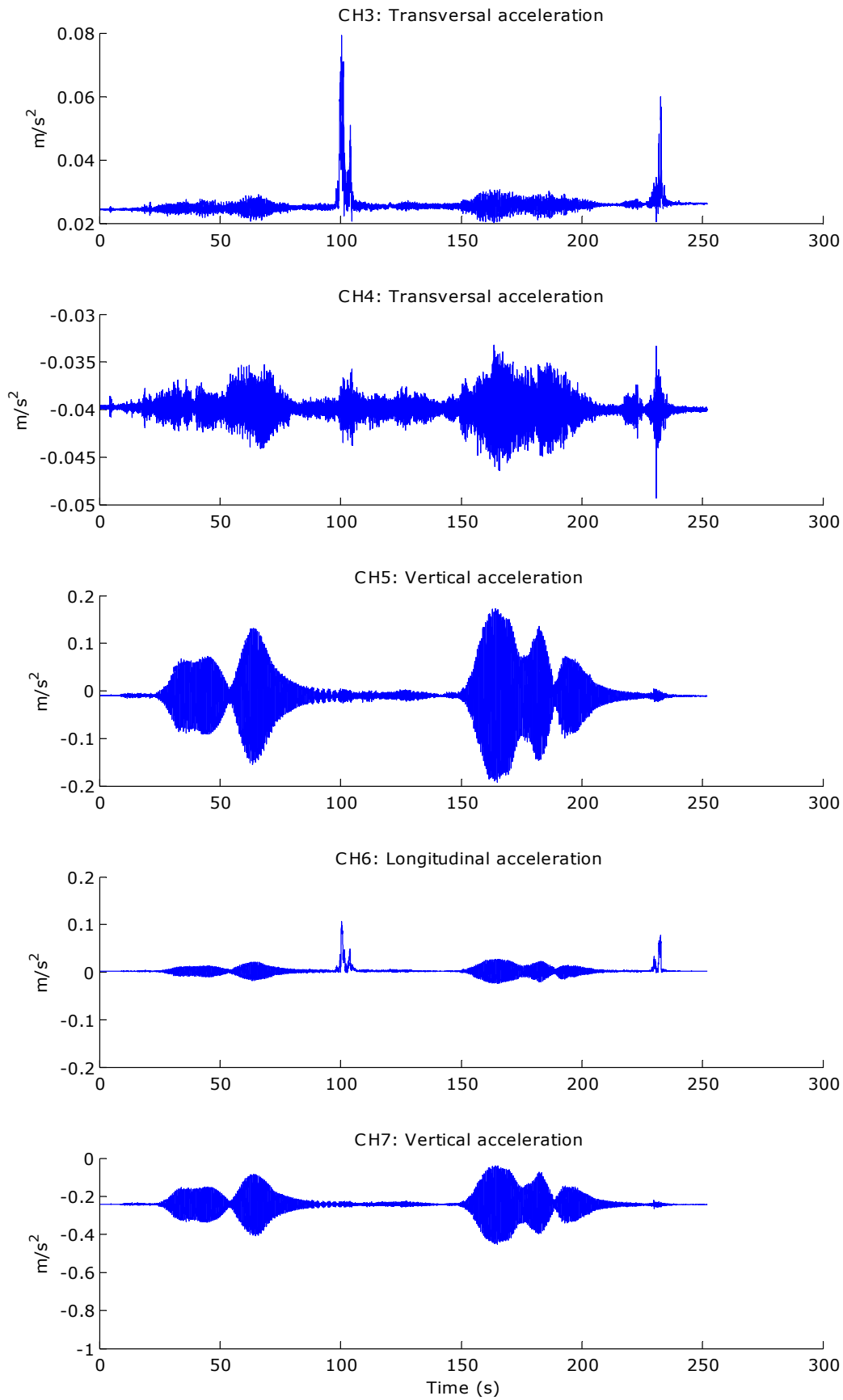
Figure C.13: Field measurement no. 13, presentation of accelerometer signals from forced excitation of the bridge.

D   Mode shapes from FE-models and modal analysis in ARTeMIS

Below follows a comparison of the natural frequencies and mode shapes between the FE-model and the modal analysis in ARTeMIS. The results from ARTeMIS primary refers to the EFDD analysis.

$f_1 = 1.01$ Hz

$f_2 = 1.78$ Hz

$f_1 = 1.62$ Hz
(*fixed bearings*)

$f_1 = 1.77 \pm 0.01$ Hz
$\xi_1 = 1.4 \pm 0.8$ %
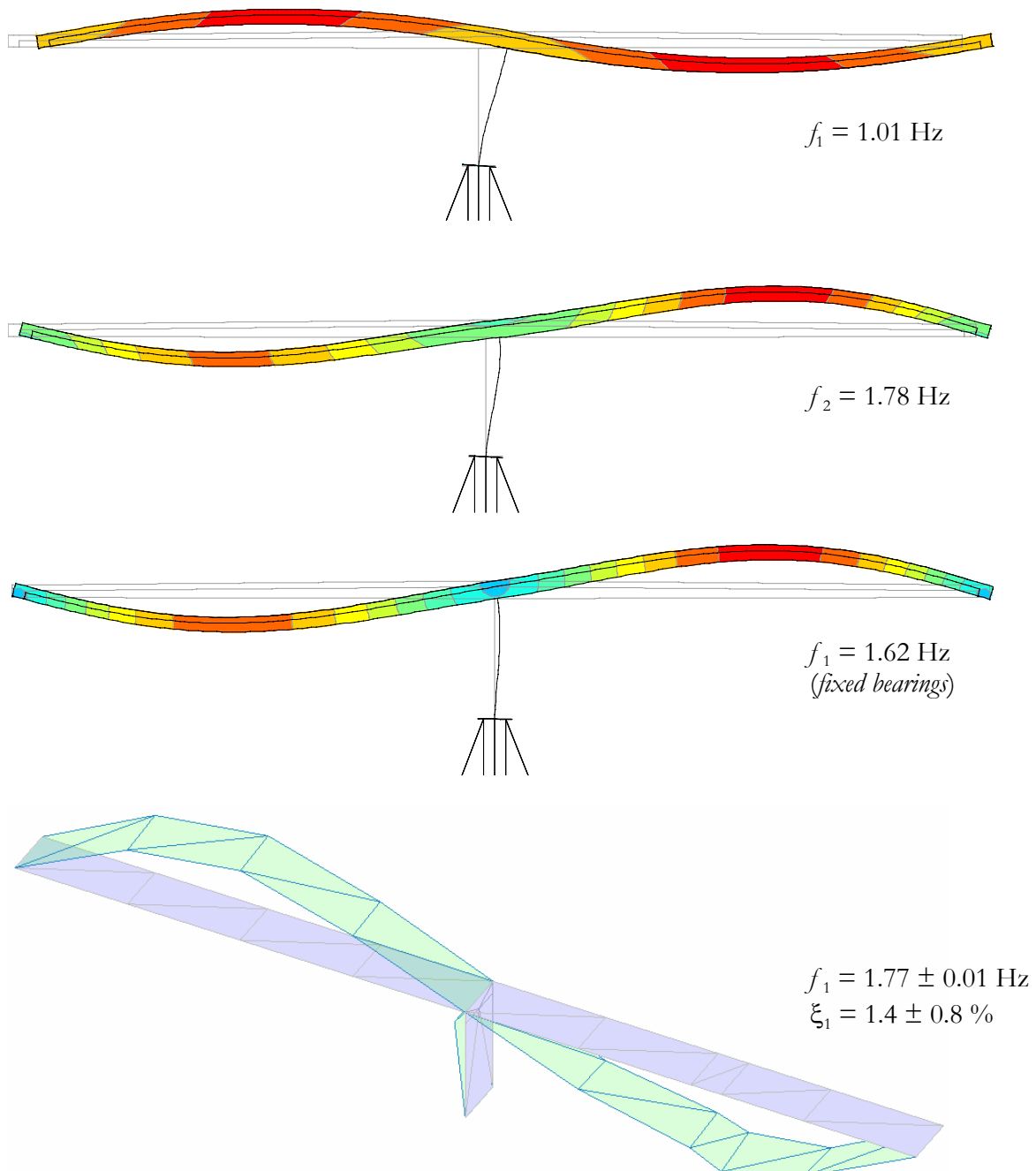
Figure D.1:   1:st antimetric vertical mode. The first mode identified in the FE-analysis have not been identified in the modal analysis, probably due to bearing friction.

f_3 = 2.14 Hz

f_3 = 2.76 Hz
(*fixed bearings*)

f_3 = 2.81 ± 0.04 Hz
ξ_3 = 0.6 ± 0.4 %
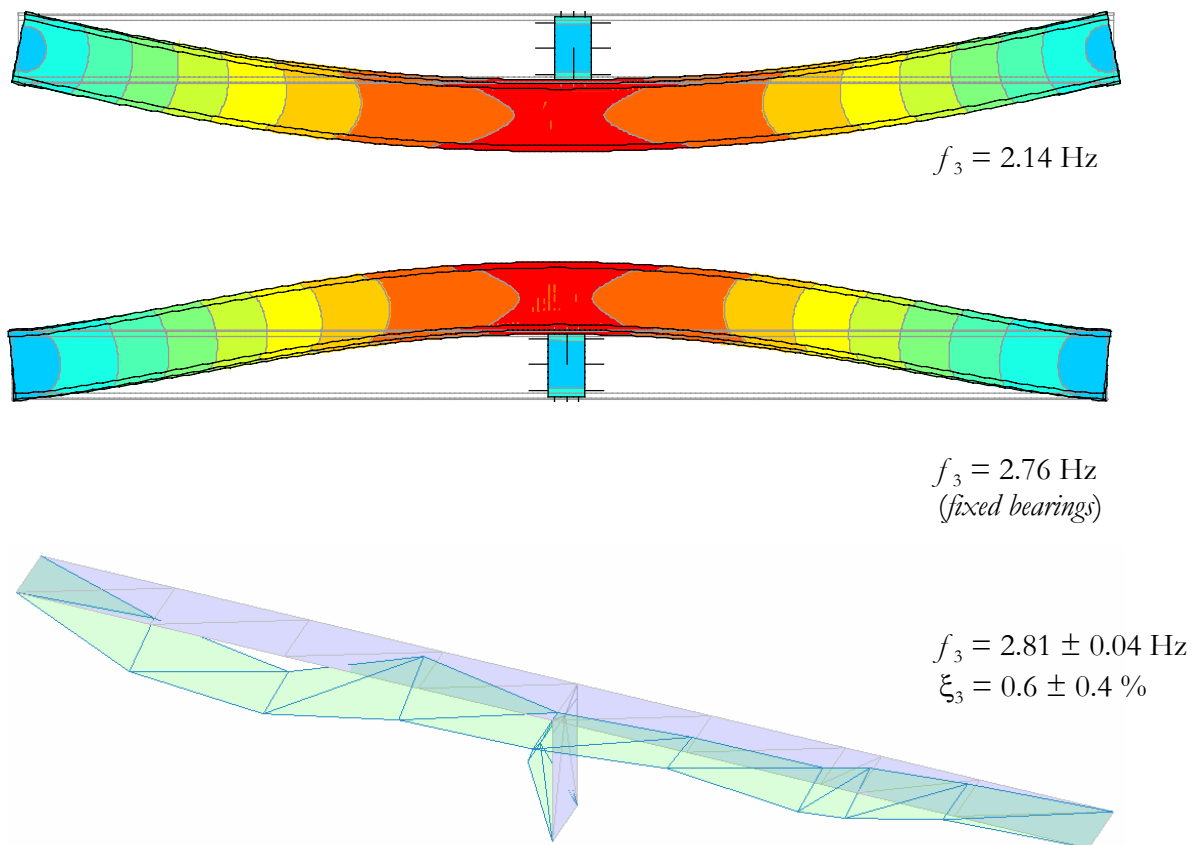
Figure D.2:   1:st transversal mode. The bearing friction results in an increase in freqeuncy from 2.14 Hz to 2.76 Hz in the FE-model. The 2:nd global mode is therby identified as the 3:rd mode, in agrrement with the modal analysis.
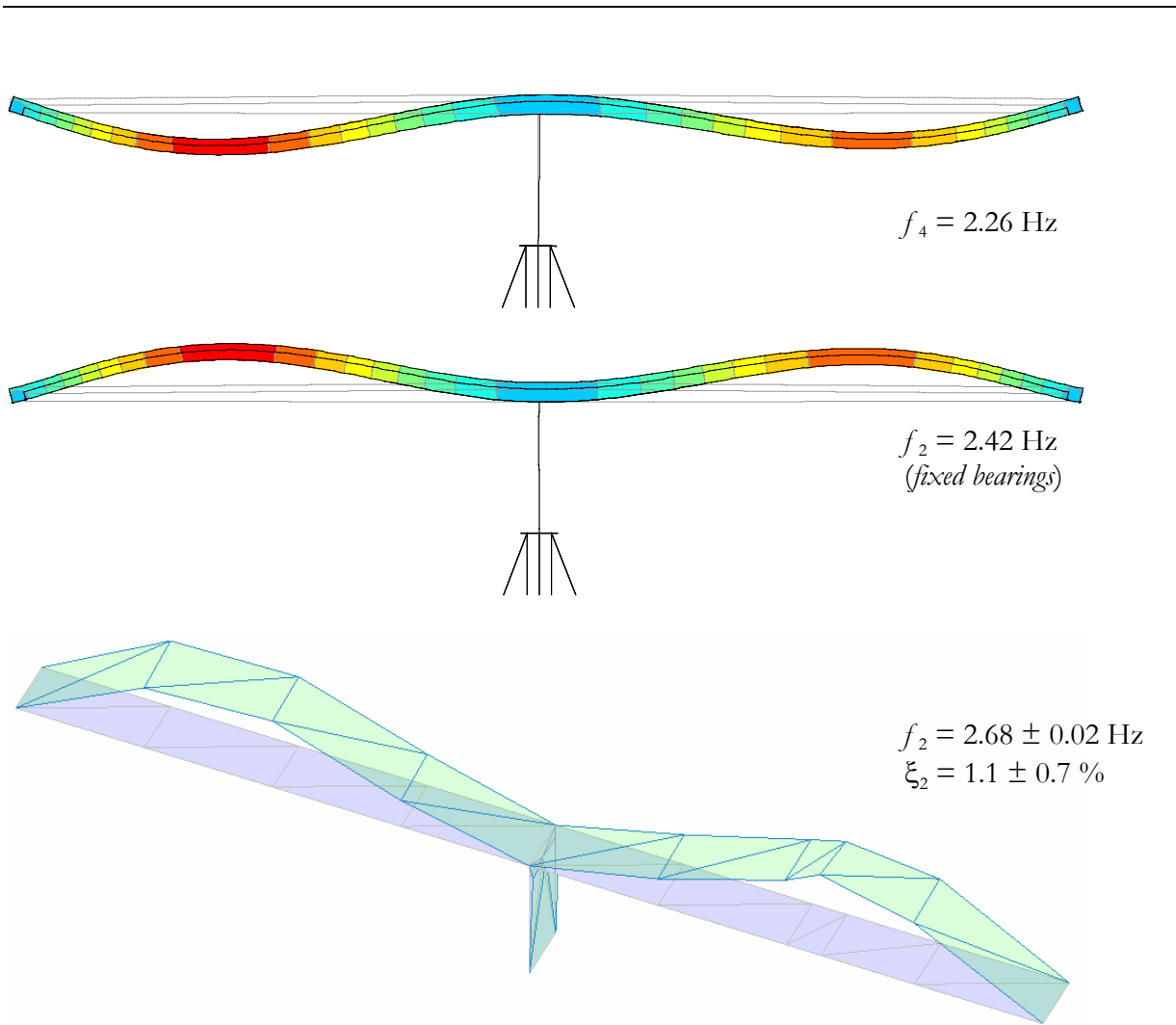
$f_4 = 2.26$ Hz

$f_2 = 2.42$ Hz
(*fixed bearings*)

$f_2 = 2.68 \pm 0.02$ Hz
$\xi_2 = 1.1 \pm 0.7$ %

Figure D.3:   1:st symstric vertical mode. The infleunce of bearing friction results in higher
frequency which corresponds to the modal analysis.

$f_5 = 4.80$ Hz

$f_5 = 5.98$ Hz
(*fixed bearings*)
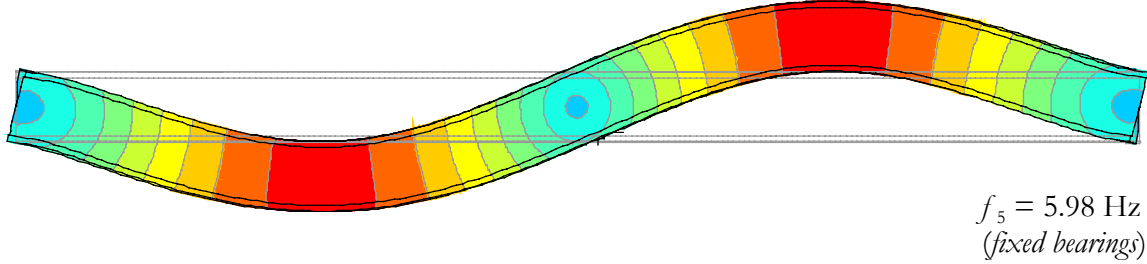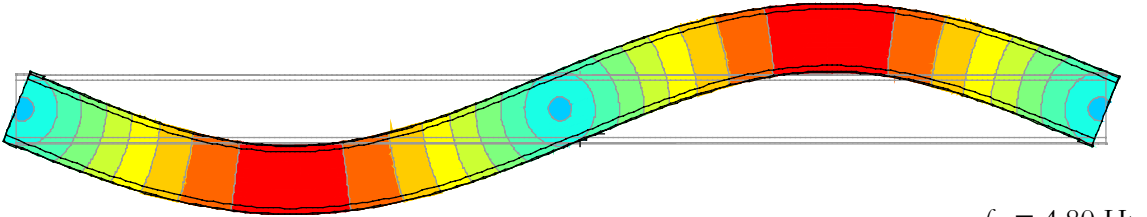
$f_4 = 5.37 \pm 0.11$ Hz
$\xi_4 = 0.7 \pm 0.4$ %
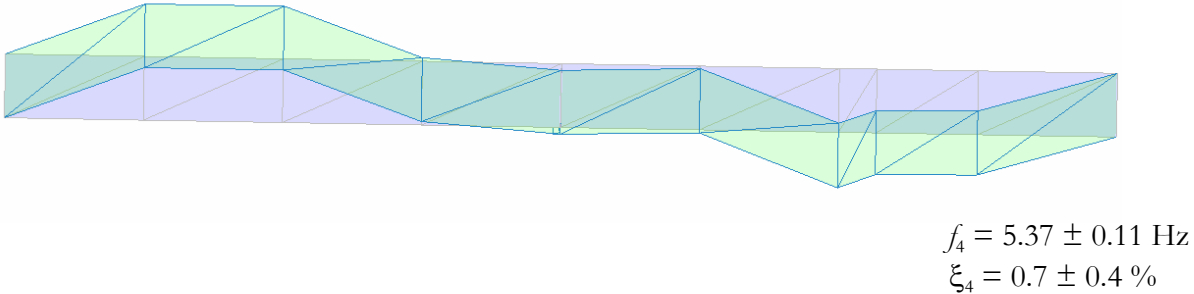
Figure D.4:   2:nd transversal mode. Fixed bearings in the FE-model results in increased natural frequency.

$f_6 = 5.67$ Hz

$f_4 = 5.51$ Hz
(*fixed bearings*)
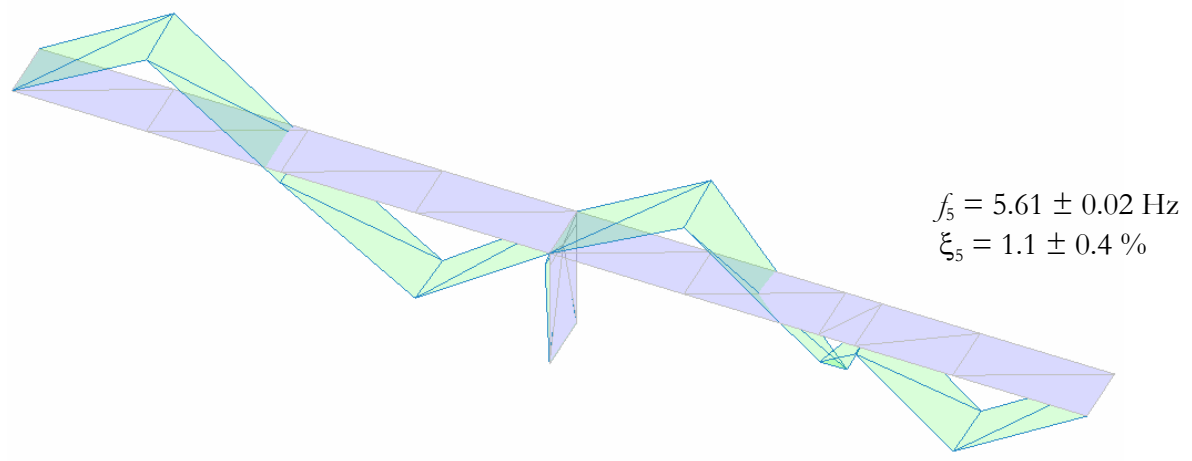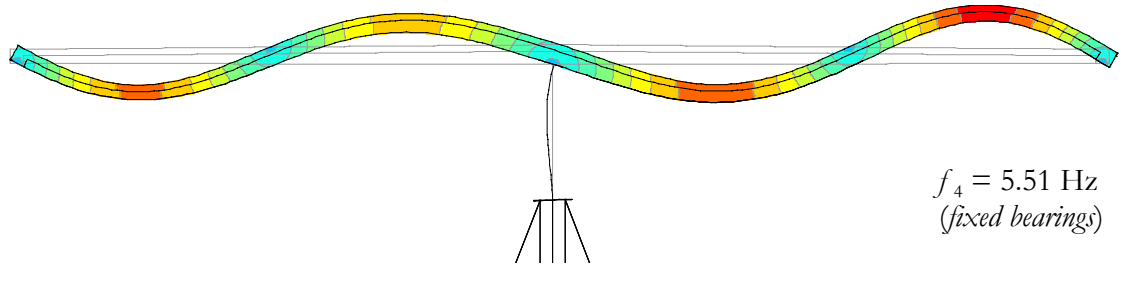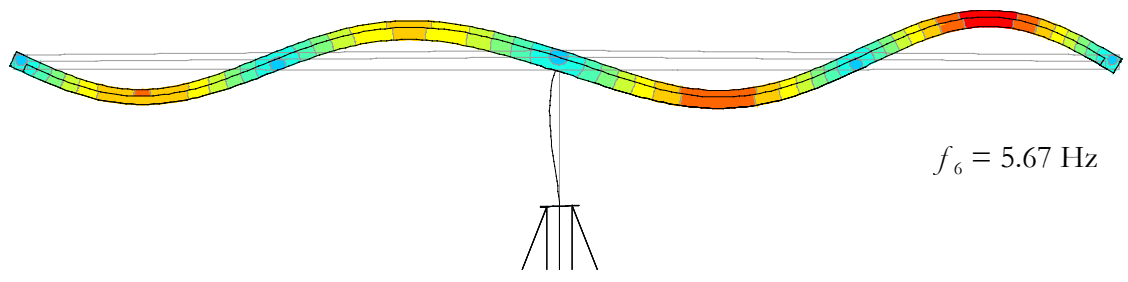
$f_5 = 5.61 \pm 0.02$ Hz
$\xi_5 = 1.1 \pm 0.4$ %

Figure D.5: 2:nd antimetric vertical mode. Bearing friction results in a small decrease in frequency. The difference is however small and both results agree with the modal analysis in both mode shape and frequency.

$f_7 = 6.89$ Hz

$f_6 = 7.11$ Hz
(*fixed bearings*)
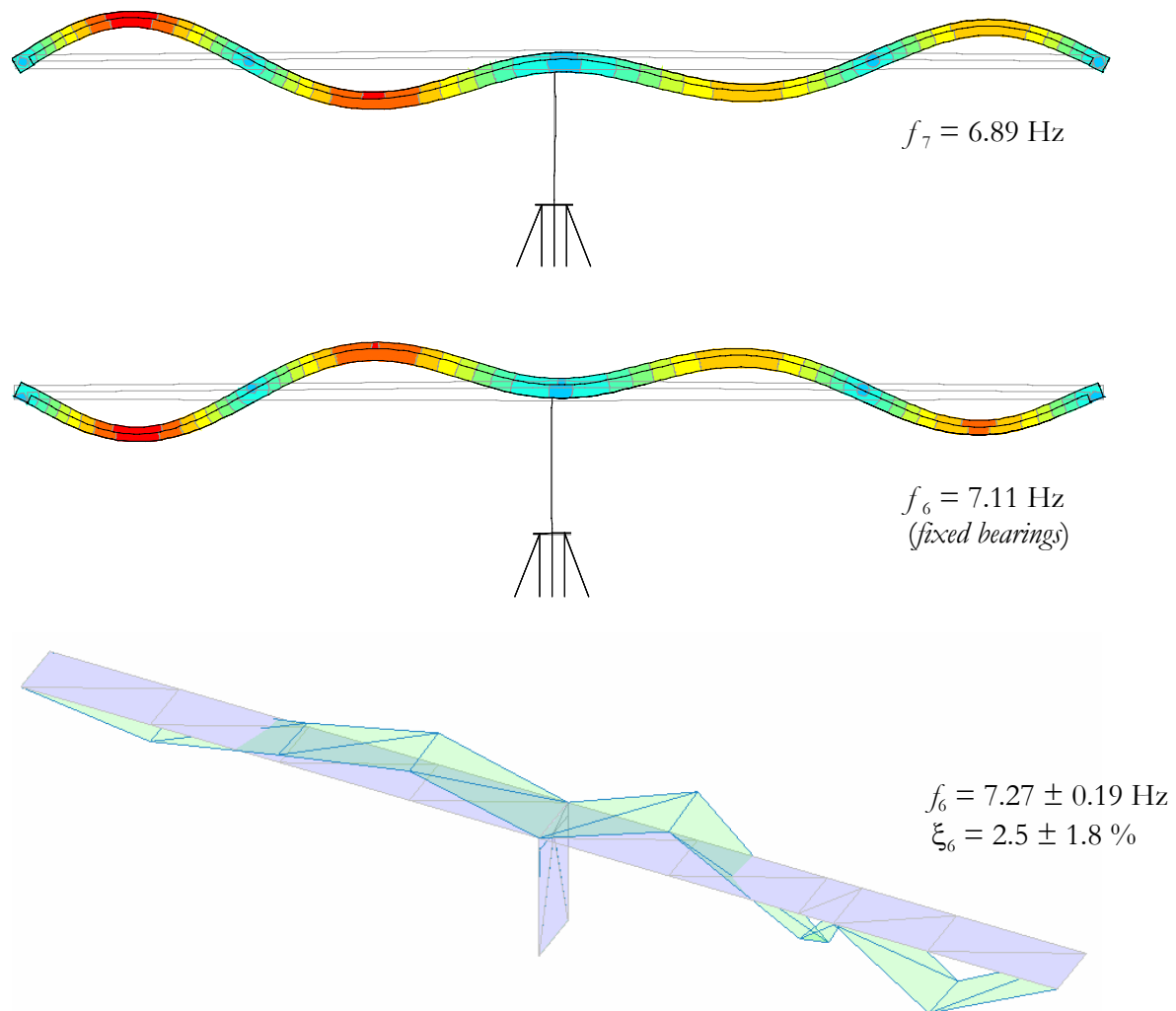
$f_6 = 7.27 \pm 0.19$ Hz
$\xi_6 = 2.5 \pm 1.8$ %

Figure D.6:   2:nd symmetric vertical mode. The influence of bearing friction is notisable and fixed bearings agree more with the modal analysis. Using the EFDD thecnique reults in relativly large standard deviation in frequency and probably an over-estimate of the damping ratio. Using the SSI methods results in more accurate results with a damping ratio about 1 %.
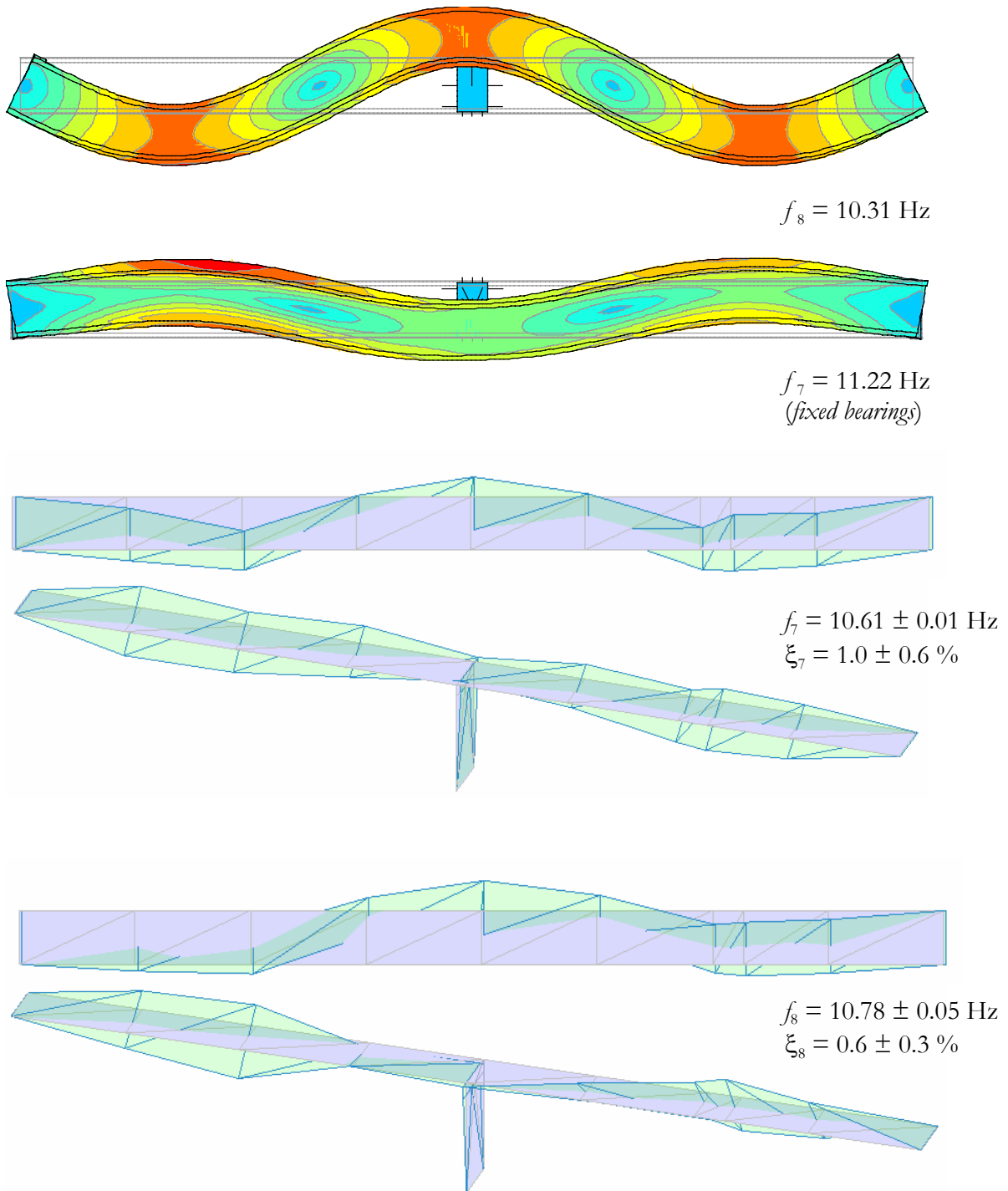
$f_8 = 10.31$ Hz

$f_7 = 11.22$ Hz
(*fixed bearings*)

$f_7 = 10.61 \pm 0.01$ Hz
$\xi_7 = 1.0 \pm 0.6$ %

$f_8 = 10.78 \pm 0.05$ Hz
$\xi_8 = 0.6 \pm 0.3$ %

Figure D.7: 3:rd transversal mode. The mode is largly influenced by torsion depending on the boundary conditions. Increased bearing friction results in more torsion and less transversal mode shape. Even if no bearing friction is concidered torsion is present, as seen as the contour ellipses in the upper figure. The modal analysis shows two coupled transversal-torsion modes, both with realistic damping ratios and standard deviations. The first candidate mode at 10.6 Hz shows in-phase torsion and the latter at 10.8 Hz off-phase torsion. If both are physical modes has not been unequivocally determined, although the torsion is in-phase in both cases in the FE-model.

$f_9 = 12.45$ Hz

$f_{10} = 12.51$ Hz
(*fixed bearings*)

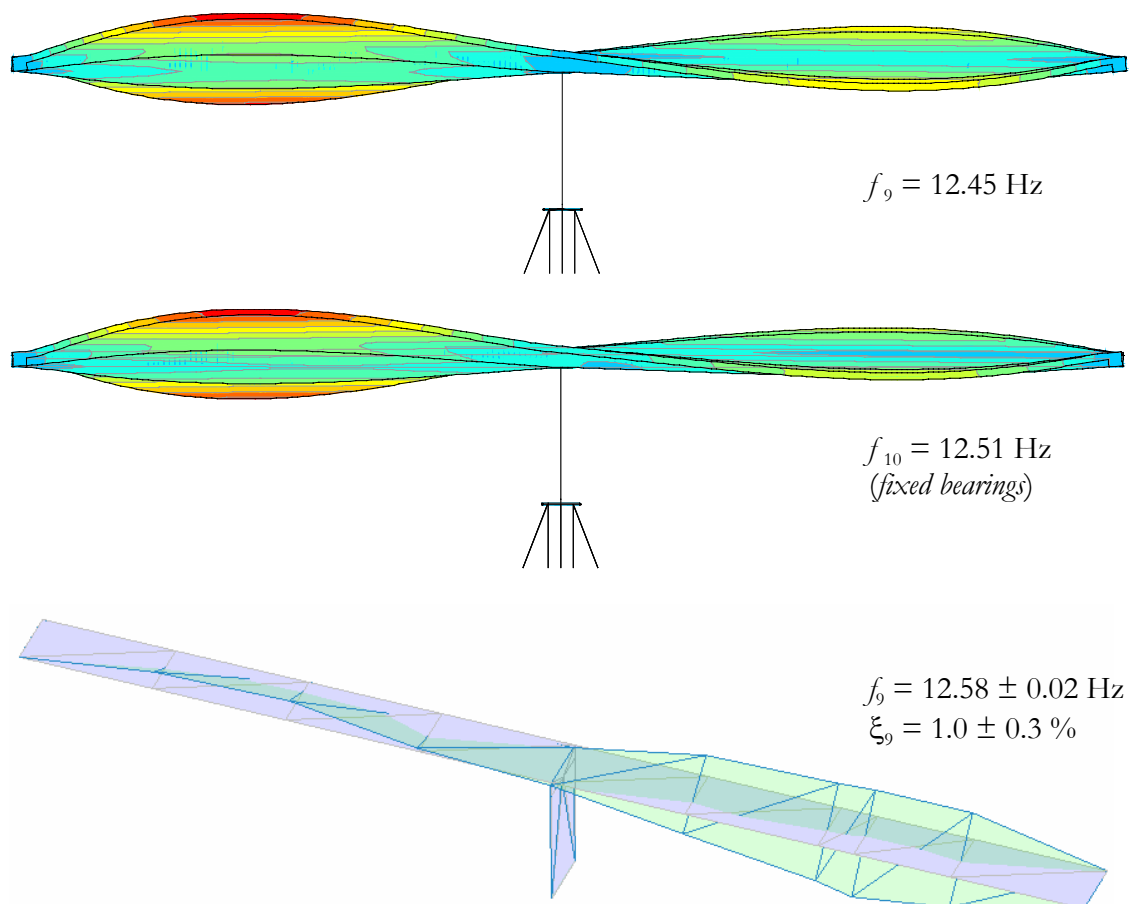$f_9 = 12.58 \pm 0.02$ Hz
$\xi_9 = 1.0 \pm 0.3$ %

Figure D.8:   1:st torsion mode. No significant influence of bearing friction can be noticed either in frequency or mode shape. The results shows good agreement with the modal analysis. Both the FE-models and the modal analysis shows a pure off-phase torsion. The estimated damping ratio is 1 % both using EFDD and all of the SSI-methods.
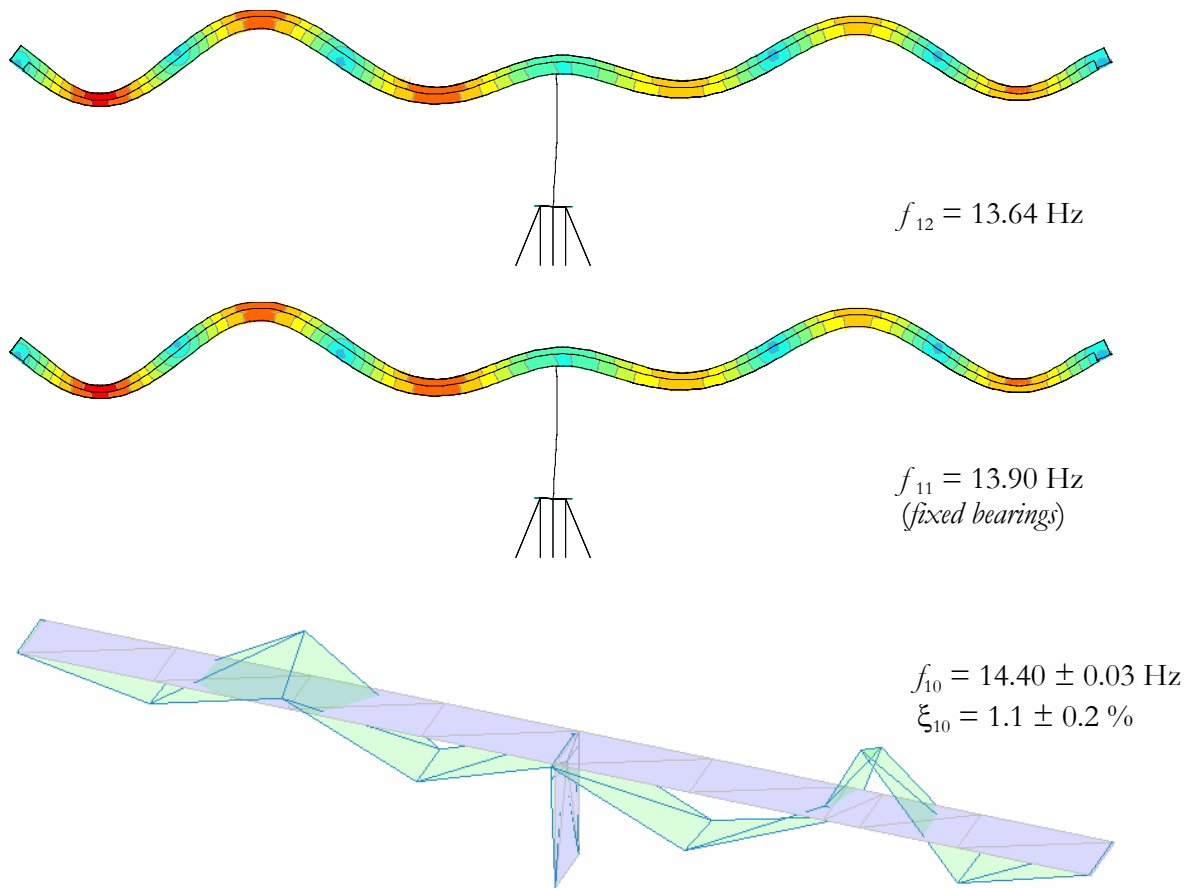
$f_{12} = 13.64$ Hz

$f_{11} = 13.90$ Hz
(*fixed bearings*)

$f_{10} = 14.40 \pm 0.03$ Hz
$\xi_{10} = 1.1 \pm 0.2$ %

Figure D.9:   3:rd symmetric vertical mode. The bearing friction has small infleunce on the symmetric mode. In the FE-model however, the 3:rd antimetric vertical mode are found at 12.06 Hz without bearing friction and at 16.56 Hz for fixed bearings. The 3:rd antimetric vertical mode has not been found from the modal analysis, probably due to insufficient number of measurement positions in order to determine this mode.